



Université du Québec
à Rimouski

**ANALYSE DE L'ÉCOULEMENT STRATIFIÉ SUR LES SEUILS DU FJORD DU
SAGUENAY**

MÉMOIRE PRÉSENTÉ

dans le cadre du programme de maîtrise en océanographie
en vue de l'obtention du grade de maître ès sciences

PAR

©[JÉRÔME GUAY]

Mai 2023

Composition du jury :

[Pierre Cauchy], président du jury, [Université du Québec à Rimouski]

[Daniel Bourgault], directeur de recherche, [Université du Québec à Rimouski]

[Cédric Chavanne], codirecteur de recherche, [Université du Québec à Rimouski]

[Peter Galbraith], examinateur externe, [Institut Maurice-Lamontagne]

UNIVERSITÉ DU QUÉBEC À RIMOUSKI

Service de la bibliothèque

Avertissement

La diffusion de ce mémoire ou de cette thèse se fait dans le respect des droits de son auteur, qui a signé le formulaire « *Autorisation de reproduire et de diffuser un rapport, un mémoire ou une thèse* ». En signant ce formulaire, l'auteur concède à l'Université du Québec à Rimouski une licence non exclusive d'utilisation et de publication de la totalité ou d'une partie importante de son travail de recherche pour des fins pédagogiques et non commerciales. Plus précisément, l'auteur autorise l'Université du Québec à Rimouski à reproduire, diffuser, prêter, distribuer ou vendre des copies de son travail de recherche à des fins non commerciales sur quelque support que ce soit, y compris l'Internet. Cette licence et cette autorisation n'entraînent pas une renonciation de la part de l'auteur à ses droits moraux ni à ses droits de propriété intellectuelle. Sauf entente contraire, l'auteur conserve la liberté de diffuser et de commercialiser ou non ce travail dont il possède un exemplaire.

« Nove sed non nova : la manière est nouvelle, mais non la matière. Citation que j'ai jamais pu replacer correctement dans une conversation. »

—Le Roi Loth d'Orcanie, Kaamelott, Livre V, tome 1, Alexandre Astier.

REMERCIEMENTS

En premier lieu, je tiens à souligner l'excellent travail de supervision de mes directeurs, Daniel Bourgault et Cédric Chavanne. L'école Bourgault-Chavanne enseigne une science humble, intègre et de haute qualité où une thèse est un moyen et non une fin. Je tiens à remercier Cynthia Bluteau pour son partage de connaissances autant scientifiques que du milieu académique. Merci à Peter Galbraith pour les sorties en mer dans le fjord. Une mention spéciale à James Caveen pour m'avoir mis sur le droit chemin numérique (Linux, Emacs). Merci à mes ami.e.s et collègues pour leur aide dans la rédaction de ce mémoire notamment : Mathilde, Jérôme, Charles-Édouard, Michel, Jean-Luc et Bruno. Finalement, merci Catherine de me supporter (dans tous les sens du terme) jour après jour. Je ne sais toujours pas pourquoi tu t'infliges ça ; Je t'aime.

Je tiens aussi à souligner le travail important de tous ceux et celles sans qui ce travail n'aurait pu être réalisé.

- Christian Boutot
- L'équipage du Coriolis II lors de la mission Sillex 2018.
- Jean-Carlos Montero Serrano
- Maxence St-Onge
- Alain Gariépy, Commandant du NGCC Amundsen, ainsi que tout son équipage.

RÉSUMÉ

Le fjord du Saguenay est une vallée glacière de 110 km de long et de 280 m de profondeur maximale qui relie la rivière Saguenay à sa tête à l'estuaire du Saint-Laurent à son embouchure. La bathymétrie du fjord est caractérisée par 3 seuils : le seuil peu profond (~ 20 m) à l'embouchure, un seuil intermédiaire (60 m) à 20 km en amont et un seuil profond (120 m) à 35 km en amont. Ces seuils séparent le fjord en 3 bassins : le bassin extérieur, le bassin intermédiaire et le bassin intérieur. La circulation dans le fjord est forcée par l'apport d'eau douce de la rivière Saguenay à sa tête, de grandes marées (jusqu'à 6 m de marnage) à son embouchure qui apportent de l'eau salée ainsi que par le vent. La circulation à grande échelle a été caractérisée par trois régimes saisonniers au cours desquels les eaux profondes, intermédiaires et de sous-surface du bassin intérieur sont renouvelées respectivement au début de l'hiver, en été et à la fin de l'hiver. Des indications indirectes suggèrent que ces régimes sont déterminés par des processus turbulents qui se produisent localement à chacun de ces trois seuils. Ici, nous présentons les résultats des expériences de terrain que nous avons menées qui visaient à étudier plus directement la dynamique des processus de seuil induits par les courants de marées ainsi que les modifications de masse d'eau qui surviennent aux seuils. À ce jour, nos mesures fournissent la description la plus précise et la plus complète des structures d'écoulement de marée stratifié autour des seuils internes du fjord du Saguenay. Nous avons également observé qu'un ressaut hydraulique interne semble se former lors de chaque marée descendante en aval du seuil intermédiaire, mais pas lors des marées montantes. Des recherches sont toujours en cours pour mieux comprendre cette asymétrie, mais notre hypothèse est que la présence d'une masse d'eau plus salée en amont du seuil intermédiaire empêche la formation d'un ressaut hydraulique, un processus qui pourrait être similaire à celui documenté à Knight Inlet (Colombie-Britannique, Canada).

Mots clés : [Fjord du Saguenay, Estuaire du St-Laurent, Processus de Seuil, Mélangé Turbulent, Océanographique Côtière]

ABSTRACT

The Saguenay Fjord is a 110 km long and 280 m deep (max depth) multi-silled glacial valley that connects the Saguenay River at its head with the St. Lawrence Estuary at its mouth. The bathymetry is characterized by 3 sills : a shallow 20-m deep sill at the mouth, an intermediate 60-m deep sill 20 km up-fjord and a deep 120-m sill 35 km up-fjord. These sills separate 3 basins, the outer, the intermediate and the inner basins. The circulation in the fjord is forced by the Saguenay River at its head that brings freshwater, large tides (up to 6 m range) at its mouth that brings salt water and by wind. The large-scale circulation has been characterized by four seasonally dependent regimes during which the deep, intermediate and subsurface waters of the inner basin are being renewed, respectively, during early winter, summer and late winter. There are indirect indications that those regimes are determined by turbulent processes occurring locally at each of these three sills. Here, we carried out field experiments to more directly investigate the detailed dynamics of tidally-driven sill processes and water mass modifications occurring across these three sills. Our measurements provide to date the most accurate and complete description of the stratified tidal flow structures around these sills. We also found that an internal hydraulic jump seems to form every ebb tide on the down-fjord side of the intermediate sill but not during flood tide on the up-fjord side. Research is ongoing to better understand this asymmetry but our hypothesis is that it is the presence of a salty pool up-fjord of the sill that prevents the formation of a hydraulic jump, a process that may be similar to that documented in Knight Inlet (British Columbia, Canada).

Keywords : [Saguenay Fjord, St-Lawrence Estuary, Sill Processes, Turbulent Mixing, Coastal Oceanography]

TABLE DES MATIÈRES

REMERCIEMENTS	vi
RÉSUMÉ	vii
ABSTRACT	viii
TABLE DES MATIÈRES	ix
LISTE DES TABLEAUX	x
LISTE DES FIGURES	xi
INTRODUCTION GÉNÉRALE	1
ARTICLE 1	
SILL PROCESSES AND RENEWAL EVENTS IN THE SAGUENAY FJORD	7
1.1 Résumé en français du premier article	7
1.2 Introduction	9
1.3 Experimental approach	18
1.4 Observations	22
1.4.1 Flow across sill B	24
1.4.2 Sill B internal hydraulic jump and internal waves	27
1.4.3 Flow across sill C	43
1.4.4 July 2018 water renewal regime	46
1.5 Interpretation	48
1.5.1 Upstream and downstream response	48
1.5.2 Internal hydraulic jump at sill B	50
1.5.3 Lateral constriction of the flow	51
1.6 Conclusion	53
CONCLUSION GÉNÉRALE	57

LISTE DES TABLEAUX

1	High and low tide times (UTC, day in parentheses) and heights for the July 2018 sill experiments, as measured from Port-Alfred, La Baie, 100 km from the mouth. A delay is to be expected between the current reversal at the sills and the tidal phase measured at La Baie. Water level data were provided by Canadian Hydrographic Service–DFO.	20
---	---	----

LISTE DES FIGURES

1	Saguenay Fjord longitudinal bathymetry. The blue shades highlight the inner, intermediate, outer basins and the Saint-Laurence Estuary which are delimited by the three sills.	10
2	Daily climatology of the Saguenay River freshwater runoff from 1944 to 2019 and 2018 daily discharge. The blue line represents the 1944-2018 daily average and the lighter blue shading is the mean plus and minus one standard deviation. The red line is 2018 data with a seven days moving average. Data were taken at the Shipshaw dam and provided by Rio Tinto.	12
3	Figure 13 from Belzile et al. (2016) . Schematic synthesis of the three types of renewal regimes in the Saguenay Fjord; (top) deep renewals during fall and early winter, (middle) mid or late winter subsurface renewals, and (bottom) intermediate renewals during summer.	14
4	Figure 9 from Farmer and Armi (1999b) . (a)-(d) Schematic summarizing the time-dependent response for stratified flow over topography discussed in the text.	17
5	Bathymetric map of the Saguenay fjord. The transect lines are drawn in red in the close-ups of the sills along with their corresponding frame of reference for along-transect (v) and across-transect (u) velocities. Sill B transect line is 5.4 km long and Sill C is 4.25 km.	20
6	Averaged CTD profiles over the fjord inner sills. The CTD measurements were averaged over 25 hours for sill B (blue) and C (red) summer profiles and over 3 hours of ebb tide for the sill B winter profiles (black). The shading correspond to the standard deviation from the average.	23
7	Water level around the time of the summer (a) and winter (b) survey campaigns. Water level data were provided by Canadian Hydrographic Service–DFO and measured at Port-Alfred, La Baie.	24
8	Complete sequence of transects over sill B showing the along-track component of the flow and the density measurements. The horizontal dotted line corresponds to the surface level. Insets show the transect number, a tide gauge with the transect time-span in red, the average surface level and the time of each transect. (a) Density measurements are missing below depth of 50 m on transects 1 and 2, up-fjord of the crest on transect 6 and none are available on transects 3,4 and 5.	29

8	(Cont)	30
8	(Cont)	31
8	(Cont)	32
8	32
9	Complete sequence of transects over sill C showing the along-track component of the flow and the density measurements. The horizontal dotted line corresponds to the surface level. Insets show the transect number, a tide gauge with the transect time-span in red, the average surface level and the time of each transect.	33
9	(Cont)	34
9	(Cont)	35
9	(Cont)	36
9	36
10	Along and across transect components of the flow velocity averaged over the transects 1, 2, 21, 22, 23, 24, 41 and 42. Positive across-track velocities are outgoing.	37
11	Transect over Sill B showing the acoustic image (arbitrary units) with a color scale ranging from blue to white to green, with green representing stronger backscatter, along-transect and vertical components of the flow with vectors grouped in bins of 0 to 0.2, 0.2 to 0.4, 0.4 to 0.8 and 0.8 to 1.0 m/s and density profiles. Note that the angle of the vectors follows the vertical to horizontal aspect ratio which exaggerates the contribution of the vertical component of the flow and that the horizontal position of the highlighted density measurements doesn't correspond to their actual location. Insets show the transect number, a tide gauge with the transect time-span in red, the average surface level, the time and an arrow that indicates the direction of travel. (a) The red box correspond to the close-up shown in the top right inset. The black vertical line in the close-up indicates the location of the density profile also shown in the inset. The horizontal dotted line corresponds to the surface level. (b) Close-up of the down-fjord half of sill B. The horizontal dotted line corresponds to the surface level.	38
11	(Cont)	39
12	Along and across transect components of the flow velocity averaged over the transects 13, 14 and 34. Positive across-track velocities are outgoing.	40

- 13 Horizontally interpolated density field of the third transect of the 2020 winter survey on March 2nd 2020. The thick black lines correspond to the winter reference isopycnals that of densities of $\sigma_t = 18.5, 22.2, 23.8$ and 24.15 kg m^{-3} . The high tide was 4.2 m at 12h15 and low tide was 1.44 m at 18h30 measured at Port-Alfred, La Baie, 100 km from the mouth. The light grey line shows the track of the CTD probe and the red dots show density inversions. 41
- 14 Transect Sill B showing the acoustic image (arbitrary units) with a color scale ranging from blue to white, with white representing stronger backscatter. The vertical lines indicate the location of the density profiles of the corresponding color. The average vertical velocity fields are shown under the acoustic images with a red to blue color scale. (a) Transect 34. The vertical velocities were averaged over the first 20 m. (b) Transect 36. The vertical velocities were averaged over the first 30 m. (c) Transect 37. The vertical velocities were averaged over the first 30 m. 42
- 15 Sequences of transects over sill C showing the acoustic image (arbitrary units) with a color scale ranging from blue to white, with white representing stronger backscatter. Insets on the left show the transect number, a tide gauge with the transect time-span in red, the average surface level, the time and an arrow that indicates the direction of travel. On the top-right corner of transect 11, an inset shows the zoomed-in region in red relative to sill C. 45
- 16 Sequences of transects over sill C showing the acoustic image (arbitrary units) with a color scale ranging from blue to white to green, with green representing stronger backscatter. Insets on the left show the transect number, a tide gauge with the transect time-span in red, the average surface level, the time and an arrow that indicates the direction of travel. On the top-right corner of transect 25, an inset shows the zoomed in region in red relative to sill C. 46
- 17 Longitudinal temperature field of the Saguenay Fjord during 3-9 July 2018. The thick black lines and the labels show isopycnals. The cyan dashed lines show isohalines whose depths in the inner basin roughly correspond to those of the selected isopycnals. The longitudinal fields were interpolated from CTD profiles located 6, 17, 20, 31, 33, 52, 62, 72, 82, and 90 km from the mouth of the fjord. The CTD profiles from the sill experiments were averaged into up-fjord profiles (relative position < 0) and down-fjord profiles (relative position > 0) for both sills to remove the semi-diurnal vertical oscillation of the isopycnals resulting in ambient profiles at 17 km, 20 km, 31 km and 33 km. Similarly the profile at 6 km is the average of the 4 CTD casts carried out over 16 hours at that location. 47

18	Maximal isopycnals height difference across sills B and C for the ebb and the flood tide.	49
19	Combined acoustic images of transects 35 (right) and 36 (left) over sill B.	51
20	Transect 4 over sill C showing along-transect and vertical components of the flow with vectors grouped in bins of 0 to 0.2, 0.2 to 0.4, 0.4 to 0.8 and 0.8 to 1.0 m/s and the width of the fjord (in colors)	52
21	Cross-sectional area and depth variation (red) relative to up-fjord geometry (-2500 m to 2400 m) and depth-integrated along-transect transport (blue) for transect 4 at sill C.	53
22	Schematic synthesis of the tidal flow over sill C (left) and sill B (right).	56

INTRODUCTION GÉNÉRALE

Le fjord du Saguenay est une vallée glacière située dans l'est du Canada en région subarctique. À ce jour, le fjord a reçu beaucoup d'attention de la communauté scientifique dans différentes branches des sciences naturelles : géologie, biologie, chimie et physique. Des éditions spéciales des journaux scientifiques *La Revue des Sciences de l'eau* (2009) et *Le Naturaliste Canadien* (2018) ont été entièrement dédiées à la recherche sur le Parc Marin du Saguenay Saint-Laurent pour célébrer les 10^e et 20^e anniversaires de la création du parc respectivement. La circulation ainsi que les mécanismes de renouvellement des eaux du fjord ont notamment été le sujet de plusieurs études telles que revues dans [Galbraith et al. \(2018\)](#). Toutefois, les processus hydrodynamiques entourant les trois seuils qui caractérisent la bathymétrie du fjord demeurent presque inexplorés. Ces processus, que l'on nomme processus de seuils, sont considérés comme étant la source principale de diffusion verticale essentielle au renouvellement des eaux du fjord ([Stacey and Gratton, 2001](#); [Belzile et al., 2016](#); [Galbraith et al., 2018](#)).

Le fjord, qui est long de 110 km, large de 2 km (en moyenne) et d'une profondeur maximale de 280 m, relie la rivière Saguenay à sa tête à l'estuaire du Saint-Laurent à son embouchure. Les trois seuils du fjord sont : le peu profond d'une profondeur de 20 m à l'embouchure [seuil A], l'intermédiaire d'une profondeur de 60 m [seuil B] et le profond à une profondeur de 120 m [seuil C] à des distances de 20 et 35 km de l'embouchure respectivement. Les seuils séparent le fjord en trois bassins communément nommés le bassin extérieur, le bassin intermédiaire et le bassin intérieur. Le bassin intérieur, d'une longueur de 70 km, est le plus long des trois (figure 1). À 95 km de l'embouchure, le fjord se divise en deux : la Baie des Ha ! Ha !, d'une longueur de 10 km, et le Bras Nord où se jette la rivière Saguenay.

À l'embouchure, le premier seuil bloque l'arrivée des eaux profondes de l'estuaire du Saint-Laurent et donc contrôle l'afflux d'eau de mer dans le fjord. Le passage des eaux profondes est possible lorsque le nombre de Froude est plus grand ou égal à 1 ([Long, 1970](#)),

c'est-à-dire lorsque $\text{Fr}^2 = U^2/(N^2 H^2) \geq 1$, où N est la fréquence de flottabilité de la stratification ambiante en aval, H est la hauteur du seuil et U est la vitesse du courant barotrope en aval. En d'autres mots, lorsque l'énergie potentielle présente dans la stratification ambiante excède l'énergie cinétique du courant, seule une fraction de l'eau sous la crête du seuil est capable d'entrer dans le fjord. La profondeur sous laquelle l'eau n'est plus en mesure de surmonter le seuil se nomme hauteur de blocage (H_b). La hauteur de blocage est estimée par $H_b \sim U/N$, en supposant que la totalité de l'énergie cinétique horizontale est transformée en mouvement vertical. Au premier seuil, des grandes marées (4 m en moyenne) génèrent des courants barotropes pouvant excéder 3 m s^{-1} (Stacey and Gratton, 2001), ce qui fournit suffisamment d'énergie cinétique pour soulever de l'eau jusqu'à 100 m sous la crête du seuil (Lavoie et al., 2000). La densité de l'eau qui entre dans le fjord est donc dépendante de la variabilité saisonnière en température et salinité des couches supérieures de l'estuaire du Saint-Laurent (premiers ~ 100 m).

La circulation estuarienne résiduelle de l'estuaire du Saint-Laurent est principalement contrôlée par des gradients de salinité caractérisés par 2 couches en hiver et 3 couches en été (Galbraith et al., 2018). En hiver, une couche d'eau froide ($T < -1^\circ\text{C}$) d'environ 75 m d'épaisseur recouvre une couche de fond plus chaude ($T < 7^\circ\text{C}$). Au printemps, le réchauffement de l'eau en surface et l'augmentation de l'apport d'eau douce créent une couche additionnelle en surface. Cette nouvelle couche de surface vient piéger une couche intermédiaire froide ($T \sim 0^\circ\text{C}$ et ~ 100 m de profond), vestige de la couche supérieure de l'hiver précédent, entre 2 couches plus chaudes.

À la tête du fjord se trouve la Rivière Saguenay, qui décharge en moyenne $1500 \pm 656 \text{ m}^3 \text{ s}^{-1}$ d'eau douce (entre 1944 à 2019) ce qui en fait la principale source d'eau douce du fjord. Les moyennes journalières de décharge d'eau douce de la Rivière Saguenay sont mesurées au barrage Shipshaw près de Chicoutimi et ont été fournies par Rio-Tinto Alcan (Bruno Larouche, communication personnelle, 2019). La figure 2 montre la climatologie journalière ainsi que la moyenne journalière pour l'année 2018 de décharge d'eau douce de la Rivière

Saguenay. D'autres plus petits cours d'eau se jettent dans le fjord et contribuent à l'apport total d'eau douce. De ceux-ci, le plus important est la rivière Sainte-Marguerite Nord-Est qui se déverse près du seuil C avec un débit moyen annuel de $30 \text{ m}^3 \text{ s}^{-1}$ (1976-1990) (Bélanger, 2003). Drainville (1968) a noté l'influence locale de la rivière Sainte-Marguerite Nord-Est sur la salinité de la couche de surface. Le ruissellement d'eau douce stratifie la couche de surface du fjord (5-10 m) avec une faible salinité ($S \sim 10$) ce qui induit l'halocline principale sous laquelle se trouve des eaux plus salées ($S \sim 30$) (Drainville, 1968; Loucks and Smith-Sinclair, 1975; Therriault and Lacroix, 1975; Therriault et al., 1984).

En plus de la couche de surface saumâtre, le bassin intérieur du fjord est caractérisé par trois autres couches : la couche de sous-surface (ou peu profonde) d'une épaisseur allant jusqu'à 50 m, la couche intermédiaire et la couche profonde qui ont toutes les deux une épaisseur d'environ 100 m (Drainville, 1968). Des analyses ont démontré que ces trois couches sont formées à 94% de la couche intermédiaire froide de l'Estuaire du Saint-Laurent et à 6% de la Rivière Saguenay (Xie et al., 2012). Bourgault et al. (2012) et Belzile et al. (2016) ont conclu que la circulation à grande échelle du fjord est caractérisée par trois régimes saisonniers durant lesquels les différentes couches du bassin intérieur sont renouvelées par l'intrusion d'eau de mélange composée d'eaux de l'estuaire du Saint-Laurent et de la Rivière Saguenay. Le renouvellement de la couche profonde se produit au début de l'hiver lorsque suffisamment d'eau dense (salée) de l'estuaire est mélangée avec de l'eau saumâtre de la couche de surface formant une masse d'eau froide et salée qui coule au fond du bassin intérieur. En coulant, l'eau plus dense fait remonter l'eau résidente de la couche profonde vers la tête du fjord qui à son tour pousse l'eau intermédiaire vers l'embouchure du fjord ce qui forme une circulation estuarienne (figure 3). Vers la fin de l'hiver, la salinité de la couche de surface de l'estuaire diminue ce qui produit un mélange d'eau moins dense. Cette eau moins dense vient remplacer l'eau de sous-surface donnant lieu à une circulation estuarienne inverse (Stacey and Gratton, 2001). Finalement, en été, l'eau chaude de la couche de surface à l'embouchure du fjord est mélangée avec l'eau de la couche intermédiaire froide de l'estuaire. Le mélange d'eau qui en découle est plus léger que l'eau de fond, mais plus lourd que

l'eau de sous-surface. Cette masse d'eau chaude vient alors s'introduire à mi-profondeur (~ 100 m) entre la couche profonde et la couche de sous-surface du bassin intérieur formant la couche intermédiaire du Saguenay. À proximité des seuils, la couche intermédiaire chaude remonte près de la surface et, combinée à l'énergie mécanique de marée, empêche la formation de glace en hiver et cause une polynie sur les 40 premiers km du fjord. Le reste du fjord est couvert de glace l'hiver à l'exception du chenal de 20 m ouvert par la Garde Côtière Canadienne. En hiver, le couvert de glace vient limiter le forçage par le vent ainsi que les transferts de chaleur avec l'atmosphère. De plus, il a été observé que le vent qui souffle sur l'estuaire peut momentanément altérer la circulation du fjord en accumulant de l'eau douce près de l'embouchure du fjord ce qui réduit la salinité de l'eau de mélange (Bélanger, 2003).

Le mélange turbulent dans le bassin intérieur joue un rôle important dans le renouvellement des eaux du fjord, car il réduit la densité de l'eau résidente profonde tout au long de l'année ce qui permet à une nouvelle eau plus dense de prendre sa place. Le renouvellement profond peut également se produire en été ou en automne si la densité de l'eau de fond de l'hiver précédent a suffisamment diminué (Bélanger, 2003; Belzile et al., 2016). Toutefois, la source du mélange turbulent dans le bassin intérieur demeure incertaine. Les taux de diffusion mesurés dans le bassin intérieur sous 50 m de profondeur sont environ un ordre de grandeur plus élevés, à $\sim 10^{-4} \text{ m}^2 \text{ s}^{-1}$, comparativement à ceux mesurés dans l'estuaire à des profondeurs similaires (Bourgault et al., 2012; Belzile et al., 2016; Cyr et al., 2011). La présence d'un couvert de glace en hiver et des taux de diffusion plus faibles au-dessus de 30 m de profondeur excluent la turbulence induite par le vent comme responsable des taux de diffusion plus élevés en profondeur (Belzile et al., 2016). En paramétrisant la diffusion turbulente comme étant inversement proportionnelle à une certaine puissance de la fréquence de flottabilité (Gargett and Holloway, 1984; de Young and Pond, 1988; Stigebrandt and Aure, 1989), Belzile et al. (2016) suggèrent que le déferlement d'ondes internes puisse être responsable des taux de diffusion plus élevés en profondeur. Des ondes internes générées au troisième seuil seraient en mesure de se propager loin dans le bassin intérieur avant de déferler et générer du mélange loin de la source d'énergie.

Les processus de seuil ont été étudiés dans plusieurs autres fjords, notamment le seuil de la baie Knight (Colombie-Britanique, Canada). Le seuil de la baie Knight est d'un intérêt particulier pour nous en raison des similarités avec le seuil B du Fjord du Saguenay en termes de la profondeur de seuil (~ 60 m) et de la vitesse des courants de marée (>1 m s $^{-1}$) ([Farmer and Armi, 1999b](#)). [Farmer and Armi \(1999b\)](#) fournit une analyse complète de la réponse temporelle de l'écoulement stratifié sur le seuil de la baie Knight. Lorsque le forçage barotrope commence, l'écoulement stratifié accélère et monte le long de la pente du seuil. Conséquemment, les vitesses de surface et de sous-surface deviennent cisaillées et la limite inférieure de la pycnocline s'enfonce. Au-dessus de la crête du seuil, le cisaillement des vitesses génère des instabilités à petite échelle (avec des amplitudes de 1-5 m, figure (4a)). Ces instabilités forment alors une interface d'entraînement qui vient progressivement incorporer de l'eau de l'écoulement stratifié sous-jacent. L'entraînement d'eau fait donc épaisser la pycnocline et forme une couche d'eau faiblement stratifiée à la crête du seuil (4b). Bien que de l'eau quitte la couche faiblement stratifiée plus en aval, les taux d'entraînements plus élevés à l'interface font que la couche faiblement stratifiée gagne en profondeur et s'étend vers l'aval (4c). L'approfondissement de la couche faiblement stratifiée permet l'incorporation d'isopycnies plus profondes menant à plus d'entraînement. Dans les premières phases de la marée, l'écoulement stratifié se détache de la pente du seuil, mais est poussé vers le bas par l'expansion de la couche faiblement stratifiée (4d). À l'intérieur de la couche faiblement stratifiée, les isopycnies se détachent une à une de l'interface d'entraînement puis remontent la colonne d'eau avant de retourner à l'horizontal plus en aval. Lorsque la couche faiblement stratifiée devient plus profonde que la crête du seuil, l'écoulement stratifié est forcé d'accélérer vers le bas le long de la pente du seuil. L'écoulement descendant devient alors rapidement supercritique ($Fr > 1$) menant à un écoulement contrôlé hydrauliquement. Un ressaut hydraulique se forme environ 300 m en aval de la crête du seuil à l'endroit où l'écoulement passe d'un état supercritique à sous-critique ($Fr < 1$) et déferle peu de temps après. Vers la fin du jusant, le forçage barotrope faiblit et l'interface d'entraînement s'enfonce à la crête du seuil. Lorsque le forçage barotrope a suffisamment diminué, le ressaut hydraulique meurt et la couche faiblement

stratifiée se déplace en amont.

[Farmer and Armi \(1999b\)](#) soulignent que les instabilités à petite échelle ne sont pas une importante source de mélange. Toutefois, de plus grandes instabilités grossissent en se déplaçant le long de l'interface d'entraînement puis contribuent au mélange local lorsqu'elles déferlent. Certaines de ces plus grandes instabilités peuvent aussi s'échapper en amont de l'interface d'entraînement pour se propager au niveau de la pycnocline sous la forme d'ondes internes ([Farmer and Armi, 1999a,b](#)). Toutefois, la majorité du mélange turbulent vient du déferlement du ressaut hydraulique ([Farmer and Armi, 1999b](#)). L'étude de [Klymak and Gregg \(2003\)](#) a aussi montré qu'une masse d'eau salée, de l'eau plus dense d'un côté du seuil, peut retarder ou encore entièrement empêcher la formation d'un ressaut hydraulique puisque la masse d'eau salée doit initialement être poussée en aval pour qu'un écoulement descendant puisse se former.

Dans l'étude de [Belzile et al. \(2016\)](#), les événements de renouvellement profond, intermédiaire, et de sous-surface surviennent respectivement au début de l'hiver, à l'été ainsi qu'à la fin de l'hiver. Toutefois, une récente étude a depuis démontré que les différents régimes de renouvellement peuvent prendre place à différents moments dans l'année ([Galbraith et al., 2018](#)). Des indications indirectes suggèrent que la chronologie des épisodes de renouvellements pourrait aussi être déterminée par des processus turbulents qui se produisent localement à proximité de chacun des trois seuils du fjord. C'est dans ce contexte que nous avons entrepris deux campagnes d'échantillonnages, une en été et l'autre en hiver, afin d'étudier directement les processus de seuil qui se produisent aux deux seuils intérieurs du fjord (seuils B et C), dynamiquement différents, et comment les propriétés physiques de la colonne d'eau sont affectées.

ARTICLE 1

SILL PROCESSES AND RENEWAL EVENTS IN THE SAGUENAY FJORD

1.1 Résumé en français du premier article

Le fjord du Saguenay est une vallée glacière de 110 km de long et de 280 m de profondeur maximale qui relie la rivière Saguenay à sa tête à l'estuaire du Saint-Laurent à son embouchure. La bathymétrie du fjord est caractérisée par 3 seuils : le seuil peu profond (~ 20 m) à l'embouchure, un seuil intermédiaire (60 m) à 20 km en amont et un seuil profond (120 m) à 35 km en amont. Ces seuils séparent le fjord en 3 bassins : le bassin extérieur, le bassin intermédiaire et le bassin intérieur. La circulation dans le fjord est forcée par l'apport d'eau douce de la rivière Saguenay à sa tête, de grandes marées (jusqu'à 6 m de marnage) à son embouchure qui apportent de l'eau salée ainsi que par le vent. La circulation à grande échelle a été caractérisée par quatre régimes saisonniers au cours desquels les eaux profondes, intermédiaires et de sous-surface du bassin intérieur sont renouvelées respectivement au début de l'hiver, en été et à la fin de l'hiver. Des indications indirectes suggèrent que ces régimes sont déterminés par des processus turbulents qui se produisent localement à chacun de ces trois seuils. Ici, nous présentons les résultats des expériences de terrain que nous avons menées qui visaient à étudier plus directement la dynamique des processus de seuil induits par les courants de marées ainsi que les modifications de masse d'eau qui surviennent aux seuils. À ce jour, nos mesures fournissent la description la plus précise et la plus complète des structures d'écoulement de marée stratifié autour des seuils internes du fjord du Saguenay. Nous avons également observé qu'un ressaut hydraulique interne semble se former lors de chaque marée descendante en aval du seuil intermédiaire, mais pas lors des marées montantes. Des recherches sont toujours en cours pour mieux comprendre cette asymétrie, mais notre hypothèse est que la présence d'une masse d'eau plus salée en amont du seuil intermédiaire.

diaire empêche la formation d'un ressaut hydraulique, un processus qui pourrait être similaire à celui documenté à Knight Inlet (Colombie-Britannique, Canada).

1.2 Introduction

The Saguenay Fjord is a multi-silled glacial valley located in subarctic eastern Canada. It has received considerable attention from the oceanography community. For example, special editions in *La Revue des Sciences de l'eau* (2009) and *Le Naturaliste Canadien* (2018) were entirely dedicated to research carried out in the Saguenay St-Lawrence Marine Park to celebrate the 10th and 20th anniversaries of the park creation. The fjord circulation and renewal mechanisms, in particular, have been the subject of many studies over the years as reviewed by [Galbraith et al. \(2018\)](#). However, the detailed physical processes occurring around the three sills that characterize the bathymetry of this fjord remain relatively unexplored. These processes, known as sill processes, are believed to be the main sources of vertical mixing driving the Saguenay water renewals ([Stacey and Gratton, 2001](#); [Belzile et al., 2016](#); [Galbraith et al., 2018](#)).

The fjord, which is 110 km long, 280 m deep (max depth) and 2 km wide (on average), connects the Saguenay River at its head with the St. Lawrence Estuary [SLE] at its mouth. The fjord's three sills are; the shallow 20 m deep at the mouth [sill A], the intermediate 60 m deep [sill B] and the 120 m deep [sill C] respectively 20 and 35 km up-fjord. The sills separate the fjord into 3 basins which are commonly referred to as the outer, the intermediate and the inner basins respectively. The inner basin, 70 km long, is the longest of the three (figure 1). 95 km from the mouth, the fjord splits into two channels ; the Ha! Ha! Bay, about 10 km long, and the North Arm where the Saguenay River connects.

At the mouth, the first sill blocks deep isopycnals in the SLE from entering the fjord thus controlling the inflow of seawater. However, deep isopycnals are able to pass over the first sill when the overall Froude number is greater or equal to one ([Long, 1970](#)), that is when $Fr^2 = U^2/(N^2 H^2) \geq 1$, where N is the buoyancy frequency of the upstream ambient stratification, H the sill height and U the upstream barotropic current velocity. In other words, when the potential energy contained in the ambient stratification exceeds the available ki-

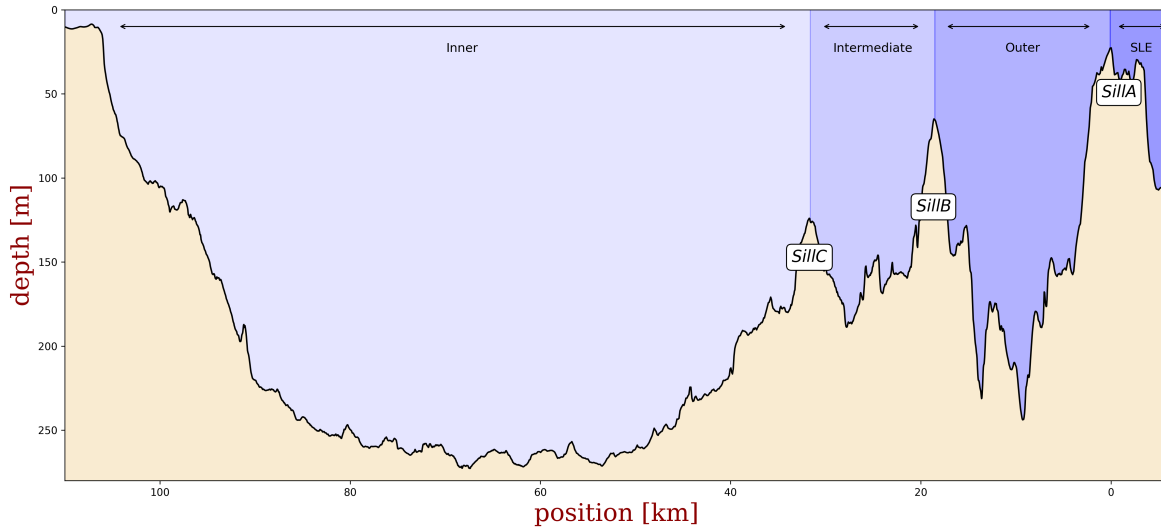


Figure 1: Saguenay Fjord longitudinal bathymetry. The blue shades highlight the inner, intermediate, outer basins and the Saint-Laurence Estuary which are delimited by the three sills.

netic energy from the current, only a fraction of the water below sill crests can make it over. The depth relative to the sill crest below which isopycnals cannot make it over is called the blocking height (H_b) and is estimated with $H_b \sim U/N$ supposing that all the available kinetic energy is converted in vertical motion. For the first sill, large tides (4 m on average) generate barotropic currents that can exceed 3 m s^{-1} (Stacey and Gratton, 2001) providing enough kinetic energy to lift isopycnals over the sill which are down to 100 m deep (Lavoie et al., 2000). The density of the waters brought in the fjord is thus controlled by the seasonal variability in temperature and salinity of the SLE upper layers (first ~ 100 m).

The residual estuarine circulation in the SLE is principally driven by salinity gradients and is characterized with 2 layers in winter and 3 layers in summer (Galbraith, 2006). In winter, a cold ($T < -1^\circ\text{C}$) layer around 75 m thick lies over a warmer ($T < 7^\circ\text{C}$) bottom layer. In spring, the warming of the surface water and the increase in freshwater discharge create an additional light surface layer. This newly-formed layer traps a cold intermediate layer [CIL] ($T \sim 0^\circ\text{C}$ and ~ 100 m deep), remnant from the previous winter upper layer, in between two

warmer layers.

At the head of the fjord, the Saguenay River is the main freshwater contributor to the fjord with a $1500 \pm 656 \text{ m}^3 \text{ s}^{-1}$ average discharge (from 1944 to 2019). The daily average freshwater discharge data were measured at Shipshaw dam near Chicoutimi and were provided by Rio-Tinto Alcan (Bruno Larouche, personal communication, 2019). It should be noted that [Bélanger \(2003\)](#) gives a lower value of $1200 \text{ m}^3 \text{ s}^{-1}$ from 1944 to 1993 with older data from Shipshaw dam. However for the same period, that is from 1944 to 1993, we obtained an average discharge of $1477 \text{ m}^3 \text{ s}^{-1}$ which differs by almost 20% from the value reported by [Bélanger \(2003\)](#). Figure 2 shows the daily climatology of the Saguenay River freshwater discharge and the 2018 daily averaged discharge. Other smaller rivers along the fjord also provide freshwater, mainly the Sainte-Marguerite Nord-Est river at an annual average rate of $30 \text{ m}^3 \text{ s}^{-1}$ (1976-1990) ([Bélanger, 2003](#)). Discharging near the third sill, [Drainville \(1968\)](#) has noted a local influence of the St-Marguerite Nord-Est river on the surface layer salinity. These freshwater runoffs stratify the surface layer of the fjord (5-10 m) with a low salinity ($S \sim 10$) inducing the main halocline below which lies saltier waters ($S \sim 30$) ([Drainville, 1968; Loucks and Smith-Sinclair, 1975; Therriault and Lacroix, 1975; Therriault et al., 1984](#)).

Apart from the surface brackish layer, the fjord inner basin is characterized by three additional layers; the sub-surface (or shallow) up to 50 m thick, the intermediate and the deep layers that are both around 100 m thick ([Drainville, 1968](#)). Analyses have shown that these three layers are composed at 94% of water from the CIL of the SLE and 6% of water from the Saguenay River ([Xie et al., 2012](#)). [Bourgault et al. \(2012\)](#) and [Belzile et al. \(2016\)](#) concluded that the large-scale circulation in the fjord is characterized by three seasonally dependent regimes during which the different layers of the inner basin are renewed by the intrusion of mixed waters formed in the intermediate and outer basins. As previously stated, these mixed waters are composed of intruding SLE water at the mouth and freshwater from the Saguenay River. Deep water are renewed in early winter when sufficiently dense (salty) water from the

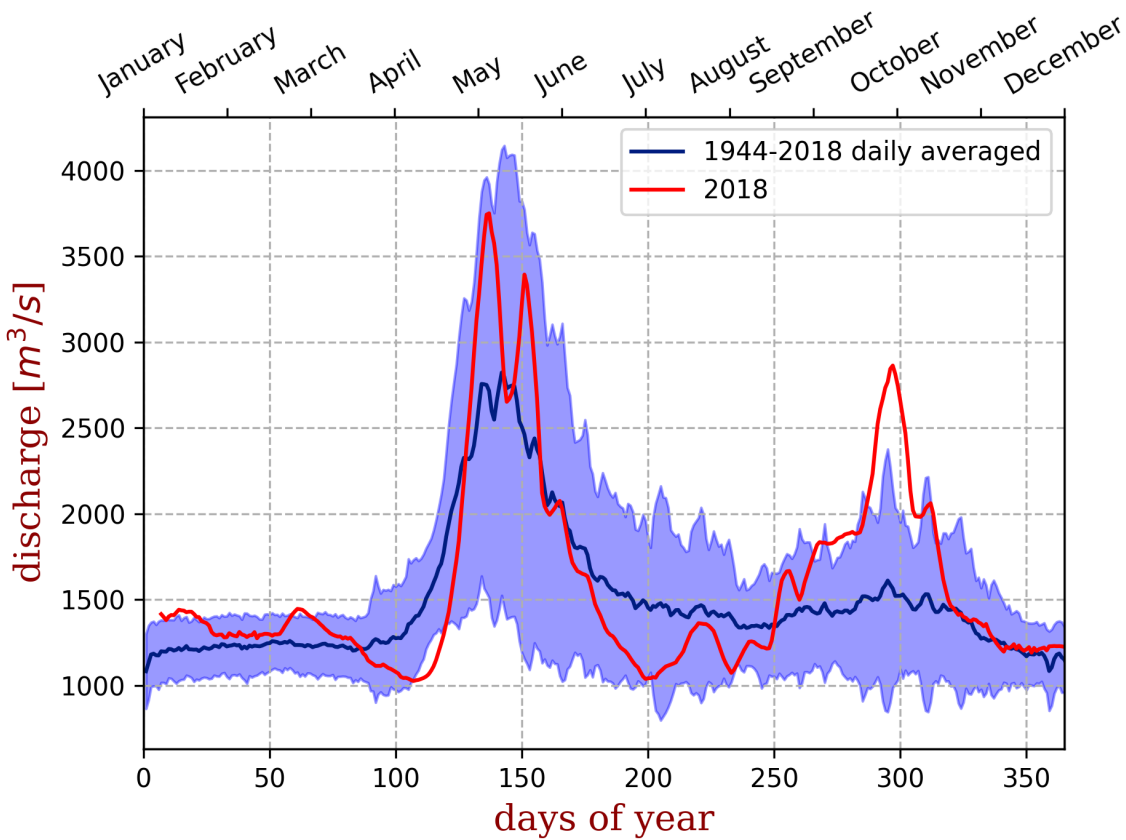


Figure 2: Daily climatology of the Saguenay River freshwater runoff from 1944 to 2019 and 2018 daily discharge. The blue line represents the 1944-2018 daily average and the lighter blue shading is the mean plus and minus one standard deviation. The red line is 2018 data with a seven days moving average. Data were taken at the Shipshaw dam and provided by Rio Tinto.

estuary mixes with a cold brackish surface layer forming a cold and salty water mass that sinks to the bottom of the inner basin. The sinking water pushes the deep resident water up towards the head of the fjord. This in turn pushes the intermediate water down-fjord creating an estuarine circulation (figure 3). In late winter, salinity decreases in the SLE upper layer forming lighter mixed waters. This results in the subsurface water being renewed in a reverse estuarine circulation (Stacey and Gratton, 2001). Lastly, in summer, warm surface waters near the fjord mouth are mixed with the estuary CIL. This generates mixed waters that are lighter than the deep water but denser than the sub-surface water resulting in a mid depth intrusion

around 100 m. These intruding warm waters compose the Saguenay intermediate layer [SIL]. In winter, the warm layer is upwelled at the sills and, combined with tidal mechanical energy, prevents ice formation and causes a polynya over the first 40 km of the fjord (Bourgault et al., 2012). The upstream portion of the fjord is ice-covered in winters, except for a 20 m wide channel kept open by the Canadian Coast Guard. The ice cover limits the forcing by the wind and the heat exchange with the atmosphere. Additionally, it was observed that wind in the estuary can momentarily alter the fjord circulation by piling up freshwater near the fjord mouth, reducing the salinity of the mixed waters (Bélanger, 2003).

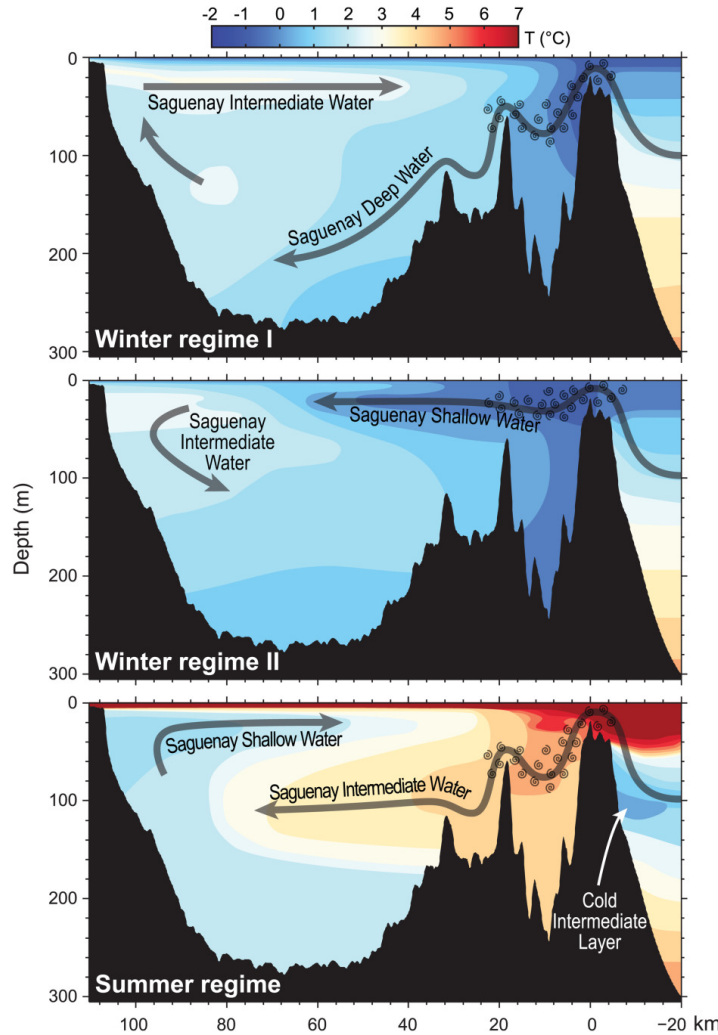


Figure 3: Figure 13 from [Belzile et al. \(2016\)](#). Schematic synthesis of the three types of renewal regimes in the Saguenay Fjord; (top) deep renewals during fall and early winter, (middle) mid or late winter subsurface renewals, and (bottom) intermediate renewals during summer.

Turbulent mixing in the inner basin plays an important role in deep water renewals as it lowers the density of the deep resident water throughout the year which then allows new denser water to take its place. Deep renewal can even occur in summer or fall if the density of deep water from the previous winter has lowered enough ([Bélanger, 2003](#); [Belzile et al., 2016](#)). However, the source of turbulent mixing in the inner basin is yet uncertain. While the

diffusion rates of $\sim 10^{-4} \text{ m}^2 \text{ s}^{-1}$ measured below 50 m in the inner basin are about one order of magnitude higher than in the SLE at equivalent depth (Bourgault et al., 2012; Belzile et al., 2016; Cyr et al., 2011), the presence of an ice cover during winter and lower diffusion rates above 30 m exclude wind induced turbulence as the source of the higher diffusion rates at depth (Belzile et al., 2016).

By parameterizing the turbulent diffusivity as being inversely proportional to some power of the buoyancy frequency (Gargett and Holloway, 1984; de Young and Pond, 1988; Stigebrandt and Aure, 1989), Belzile et al. (2016) suggested that the breaking of internal waves could be responsible for the higher diffusion rates in the inner basin. Internal waves generated at the third sill could propagate well into the inner basin before breaking, leading to mixing away from the energy source.

Sill processes have been studied in several other fjords. Notably the Knight Inlet sill (British Columbia, Canada) which has been well documented over the years. Knight Inlet sill is of special interest to us due to the similarity in sill depth with the Saguenay fjord sill B (60 m deep) and the strong (over 1 m s^{-1}) tidally induced currents (Farmer and Armi, 1999b). In Farmer and Armi (1999b) we find a comprehensive analysis of the time-dependent response of the tidally forced stratified flow over Knight Inlet sill that goes as follows. As barotropic forcing begins, the stratified flow accelerates as it moves up the sill. Consequently, the surface and sub-surface velocities become sheared and the pycnocline lower boundary deepens. Over the sill crest, the sheared velocities lead to small-scale instabilities (with amplitudes of 1-5 m, figure 4a). These instabilities form an entrainment interface that progressively incorporates water from the stratified flow underneath it. This thickens the pycnocline resulting in a slowly moving weakly stratified layer at the sill crest (figure 4b). Although some water leaves the weakly stratified layer further downstream, higher entrainment rates at the interface cause the weakly stratified layer to deepen and to extend downstream (figure 4c). The deepening of the weakly stratified layer leads to more isopycnals being incorporated in the entrainment interface and thus to more entrainment. In the first phases of the tide, the strat-

ified flow separates from the sill face, but as the weakly stratified layer deepens, the flow is diverted downward (figure 4d). Within the weakly stratified layer, isopycnals detach from the entrainment interface sloping upward and return to the horizontal further downstream. The weakly stratified layer eventually gets deeper than the sill crest forcing the stratified flow to accelerate down the sill face. The downslope flow quickly becomes super-critical ($Fr > 1$) leading to the fully established hydraulically controlled flow. An internal hydraulic jump form around 300 m downstream of the crest as the super-critical flow slows to sub-critical velocity ($Fr < 1$) and subsequently breaks. Approaching the end of the tide of the falling tide, the barotropic forcing decreases and the entrainment interface deepens at the sill crest. When the barotropic flow has sufficiently slackened, the internal hydraulic jump dies and the weakly stratified layer moves upstream in an exchange flow.

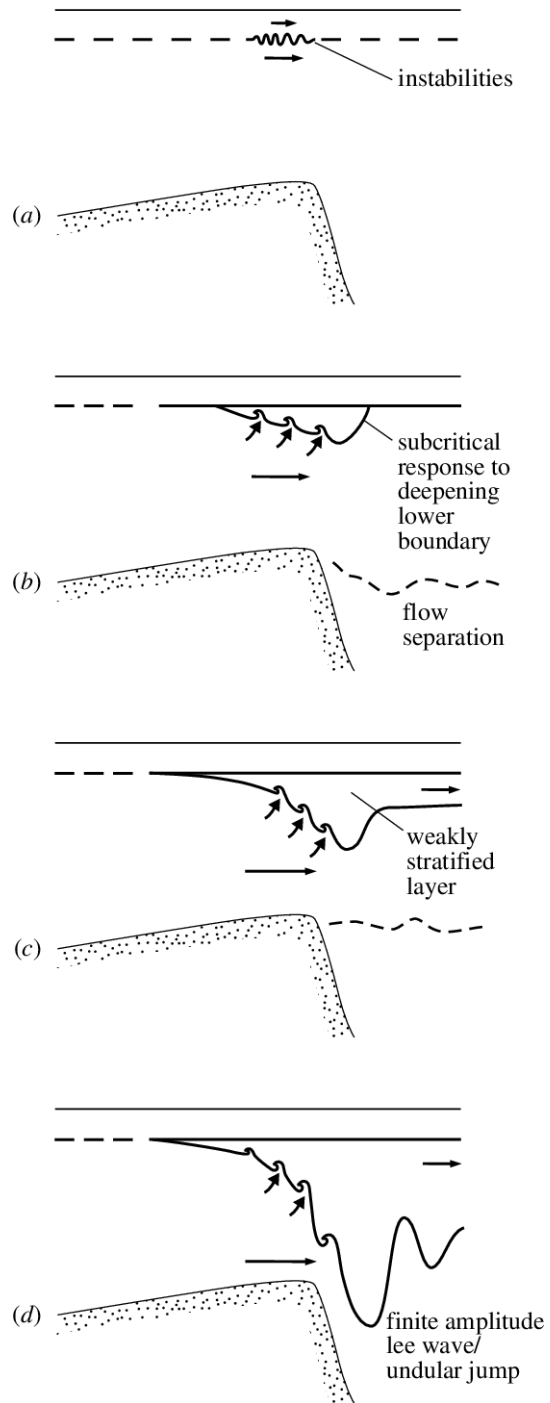


Figure 4: Figure 9 from [Farmer and Armi \(1999b\)](#). (a)-(d) Schematic summarizing the time-dependent response for stratified flow over topography discussed in the text.

[Farmer and Armi \(1999b\)](#) points out that the small-scale instabilities are not an important source of mixing. Bigger instabilities grow as they move along the entrainment interface and then contribute to local turbulent mixing when collapsing. These instabilities can also escape upstream of the entrainment interface and then propagate at the pycnocline as internal solitary waves ([Farmer and Armi, 1999a,b](#)). However, the most important source of turbulent mixing comes from the breaking of the internal hydraulic jump ([Farmer and Armi, 1999b](#)). [Klymak and Gregg \(2003\)](#) also showed that a salty pool of denser water on one side of the sill can delay or entirely suppress the formation of the internal hydraulic jump since the salty pool has to be first flushed downstream for a downslope flow to form.

In the [Belzile et al. \(2016\)](#) study, the deep, the intermediate and the sub-surface renewal events occurred respectively during early winter, summer and late winter, but annual surveys have shown since then that those regimes can happen at different times throughout the year. [Galbraith et al. \(2018\)](#) discovered a fourth regime in spring that is similar to the low salinity sub-surface renewal previously observed in late winter. Indirect indications suggest that the timing of the renewal events could also be determined by turbulent sill processes occurring locally at each of the fjord three sills. Within this context, we carried out summer and winter field experiments to investigate more directly the tidally-driven sill processes over the two dynamically different inner sills and how the water properties are affected.

1.3 Experimental approach

A summer survey campaign took place from the 3rd to the 9th of July 2018 aboard the R/V Coriolis II. The research vessel was equipped with a Teledyne 4-beams 150 kHz acoustic Doppler current profiler (ADCP) and a Simrad 38 kHz echo sounder; both were hull-mounted. The first ADCP depth cell is centered 12.25 m below sea level and each cell is 8 m thick. On board were two CTD profilers: a Seabird SBE 49 (16 Hz) mounted on a remote controlled towed platform, a Scanfish II by EIVA Marine; and a Seabird SBE 9 (24

Hz) mounted on a Rosette. The Scanfish II was towed from the ship's stern with a 500 m long cable and sampled the water column for temperature and salinity by oscillating up and down at an average vertical rate of $\pm 0.06 \text{ m s}^{-1}$. The true coordinates of the temperature and salinity measurements were computed by factoring in the depth of the Scanfish II at any given time.

The summer sill experiments consisted of two series of repeated transects carried over the sill B and C, during which the water column was continuously sampled for velocities (ADCP), acoustic backscatter images (Echo Sounder) and temperature and salinity properties (SBE 49 / Scanfish II). Each experiment lasted for 25 hours and spanned over two complete semi-diurnal tidal cycles. The sampling began at 19h25 (UTC) on July 3rd and at 22h15 (UTC) on July 4th over sill B and C respectively. The transect line at sill B extended about 3 km up-fjord and 2.3 km down-fjord of the sill crest and about 2.5 km up-fjord and 1.7 km down-fjord at sill C (figure 5). The transects took approximately 23 minutes to complete at sill B and 20 minutes at sill C with a total of 41 and 44 transects respectively. Tides charts for both experiments are presented in table 1. In addition to the sill experiments, the water column was sampled for temperature and salinity with the Rosette's CTD profiler at different distances from the mouth of the fjord: 6 km (4 times over 16 hours), 52 km, 62 km, 72 km, 82 km, 90 km.

Apart from the ADCP internal processing, quality control was carried out to flag side-lobes contaminated cells and cells with current components exceeding $\pm 1 \text{ m s}^{-1}$. A 1 m s^{-1} velocity threshold was used to remove obviously bad measurements that were not flagged by systematic quality control, which accounts for about 0.1% of the remaining north and east velocities.

A winter survey took place in March 2020 aboard the CCGS Amundsen as part of the 2020 Odyssée Saint-Laurent winter mission. The winter experiment took place on the ebb tide and consisted of three transects over the down-fjord face of sill B. Each transect was carried out starting from the sill crest and the ship oriented against the ebb flow. During

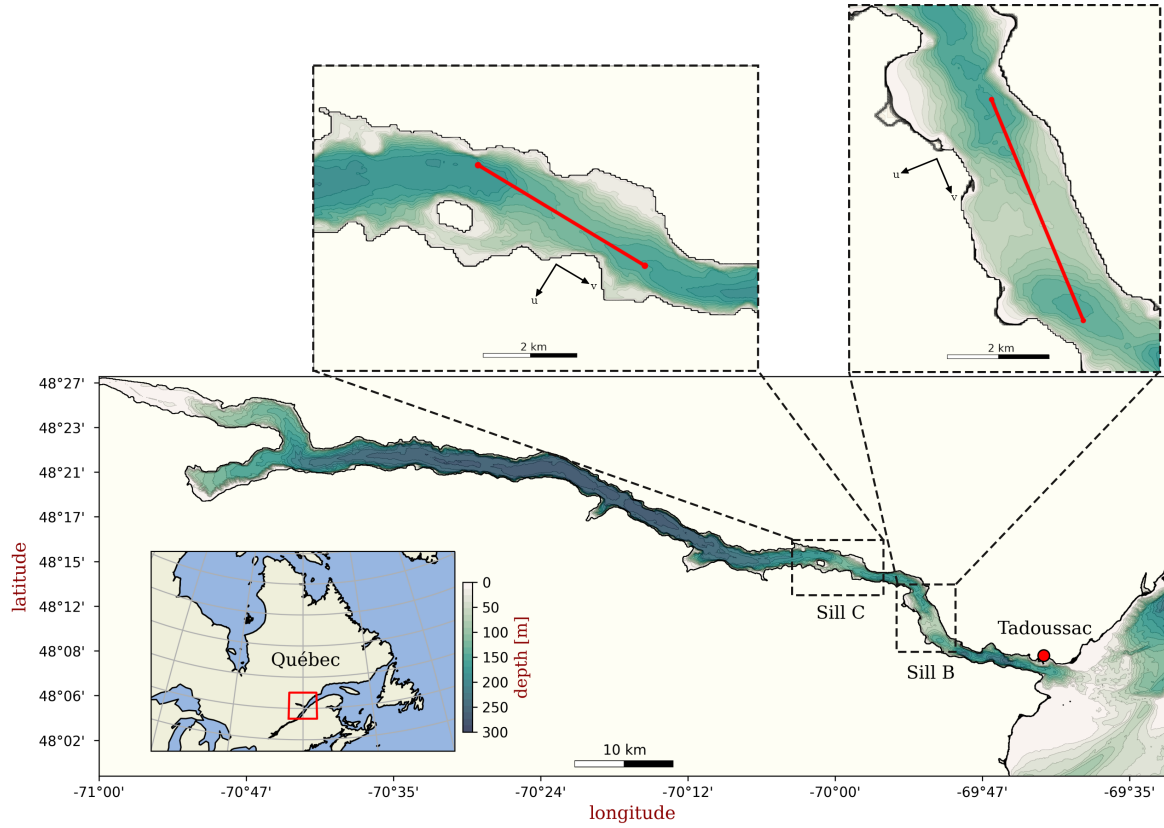


Figure 5: Bathymetric map of the Saguenay fjord. The transect lines are drawn in red in the close-ups of the sills along with their corresponding frame of reference for along-transect (v) and across-transect (u) velocities. Sill B transect line is 5.4 km long and Sill C is 4.25 km.

Table 1: High and low tide times (UTC, day in parentheses) and heights for the July 2018 sill experiments, as measured from Port-Alfred, La Baie, 100 km from the mouth. A delay is to be expected between the current reversal at the sills and the tidal phase measured at La Baie. Water level data were provided by Canadian Hydrographic Service–DFO.

Sill	Low	High	Low	High	Low	High
B	(3)17h00 0.87 m	(3)23h20 4.06 m	(4)5h15 1.20 m	(4)11h30 4.51 m	(4)18h00 1.01 m	(5)00h15 4.08 m
C	(4)18h00 1.01 m	(5)00h15 4.08 m	(5)05h55 1.35 m	(5)12h15 4.27 m	(5)18h40 1.22 m	

the transects, the water column was continuously sampled for temperature and salinity by

winching up and down a CTD profiler, a Seabird SBE19+ (4 Hz), from the bow. The first transect started 2.5 hours after the high tide and the third ended about 3 hours later. The CTD profiler was winched at a constant rate of 1 m s^{-1} resulting in an averaged horizontal resolution that varies from 100 m on top of the sill to 200 m in the deepest part. Avoiding ice floes collision with the CTD cable made it difficult for the ship to travel in a straight line and, as a result, the vessel deviated to the west on the first and second transects. The third transect was right on track and extended for an additional kilometer down-fjord.

For both surveys, the *in situ* density was computed with the Gibbs Seawater (GSW) Python package from absolute salinity and conservative temperature. The CTD profiles were then sorted such that density increased monotonically in order to have ambient stratification, that is without density inversions.

Since measurements from the repeated transects were recorded as a time series, a fixed frame of reference was needed to analyze and compare the data from different transects. The vessels GPS tracks were projected onto the fixed transect lines showed in figure 5 in order to compute positions relative to the sill crests. The axis for the frame of reference are the across-transect axis (x), the along-transect axis (y) and the vertical axis (z). The along-transect axis is set positive down-fjord and the vertical axis is set positive upward. The depths recorded by the different instruments were adjusted to indicate depth relative to bathymetric map using water level data from the tide gauge located in the Ha! Ha! Bay near La Baie. ADCP data were averaged into 50 m horizontal bins and rotated onto the transect frame of reference with along-transect and across-transect velocities components. Unfortunately, the ADCP data at the bottom were flagged as bad data by the different quality tests resulting in a 20 to 30 m thick layer where velocity data are absent.

1.4 Observations

The average density structures over each inner sill for summer and winter observations (figure 6), were computed with the CTD measurements from the repeated transects. From these profiles, we see that in summer water between depths of 10 and 20 m is slightly denser ($< 0.5 \text{ kg m}^{-3}$) at sill C but at the surface ($d < 10 \text{ m}$) is about 4 kg m^{-3} denser at sill B. In winter, the higher salinity and lower temperature lead to a slight positive shift in the average density profile at sill B compared to the summer average. Figure 7 shows that both the summer and winter observations were made approaching neap tide thus, during low-energy tide cycles. The summer observations of the tidal variability of the density and along-channel velocity across sills B and C are presented in figures 8 and 9. When discussing the observations, the terms downstream and upstream will refer to the direction of the tidal flow. The density structure is shown with colored dots that correspond to the pycnocline center ($\sigma_t = 17.0 \text{ kg m}^{-3}$, $d = \sim 5 \text{ m}$), the pycnocline lower boundary ($\sigma_t = 21.5 \text{ kg m}^{-3}$, $d = \sim 10 \text{ m}$) and the average density measured at depth of 20, 40 and 80 m ($\sigma_t = 22.25$, 23.0 , 23.6 kg m^{-3}) over both inner sills. As previously mentioned, velocity measurements are missing in the last 20 to 30 m of the water column such that the complete structure of the flow over the sills cannot be fully documented. Additionally, the twelfth transect over the sill B was not completed and is thus absent from the sequence.

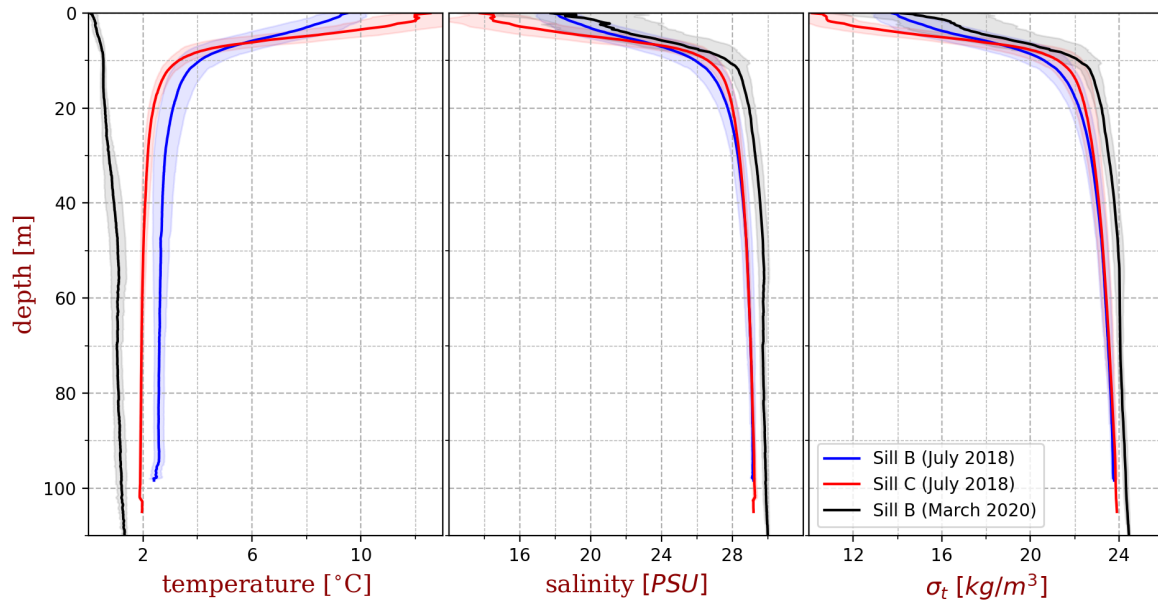


Figure 6: Averaged CTD profiles over the fjord inner sills. The CTD measurements were averaged over 25 hours for sill B (blue) and C (red) summer profiles and over 3 hours of ebb tide for the sill B winter profiles (black). The shading correspond to the standard deviation from the average.

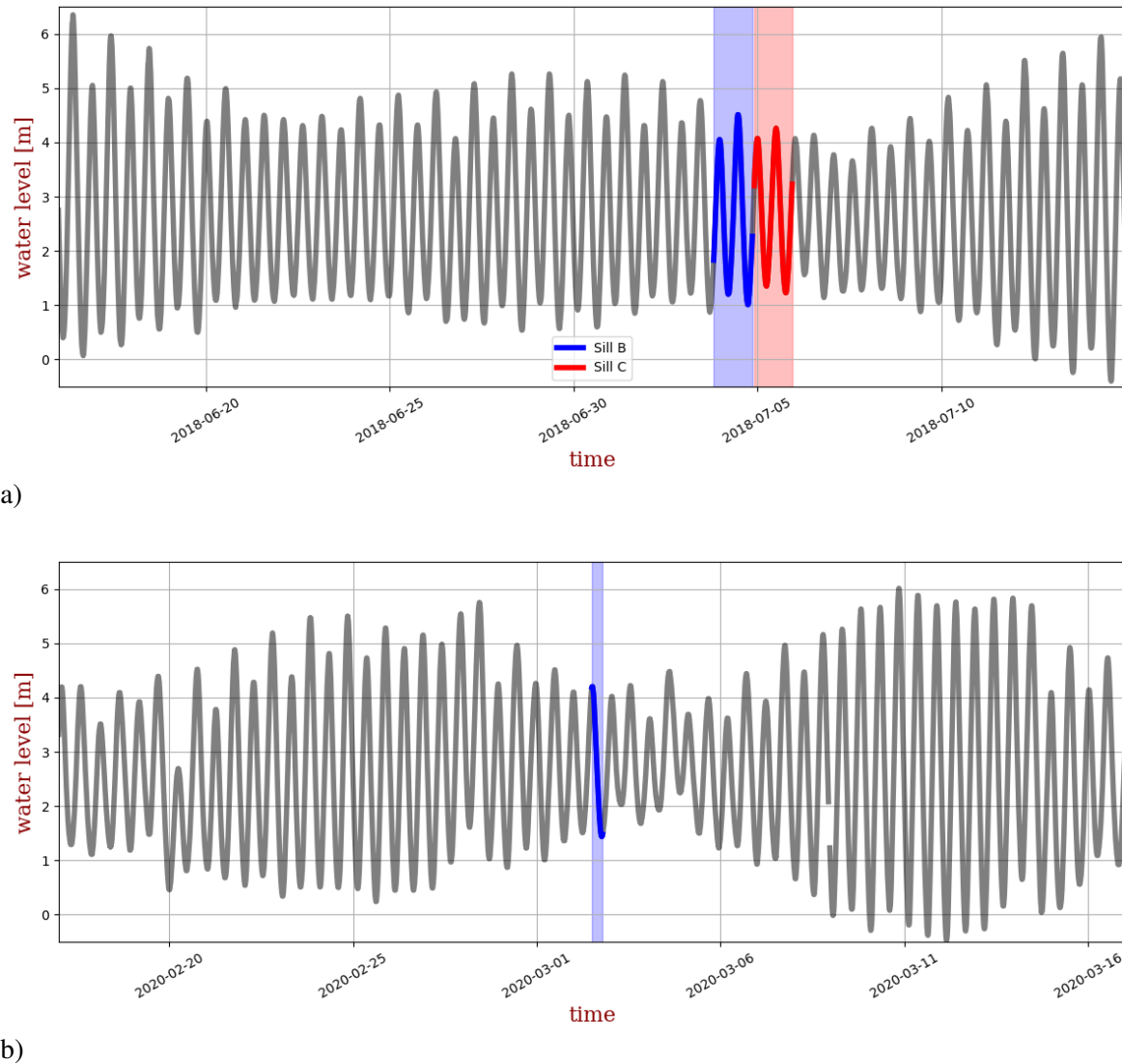


Figure 7: Water level around the time of the summer (a) and winter (b) survey campaigns. Water level data were provided by Canadian Hydrographic Service–DFO and measured at Port-Alfred, La Baie.

1.4.1 Flow across sill B

Transects 18-19 and 39 (figure 8) correspond to the time of the first and second low tide of the sequence. At the low tide, a down-fjord flow, between 0.2 and 0.4 m s^{-1} , is present

over the sill. As will be shown later, this down-fjord flow is a remnant of the previous ebb tide flow that persists sometime after the end of the barotropic forcing which indicates that the tide is at least partly progressive. Furthermore, the 22.25 kg m^{-3} , 23.0 kg m^{-3} and 23.6 kg m^{-3} isopycnals, which will be referred to as the deep isopycnals, are about 10 to 20 m higher on the up-fjord side of the sill than on the down-fjord side. The isopycnal height difference across the sill is also a remnant of the previous ebb tide forcing. In the hour following the low tide (transects 19-20 and 39-40), the remaining down-fjord current relaxes and the deep isopycnals rise up to their respective average depths. During the second hour of the flood tide (transects 21-22 and 41) water in the down-fjord basin begins to accelerate up the sill. Above the sill, the currents increase to 0.6 m s^{-1} and a 20 m thick flow begins to move down along the up-fjord slope of the sill. Two hours after the low tide (transects 23 and 42), the flow appears to separate from the sill slope about 50 m below sill depth and 1500 m up-fjord of the crest. As the barotropic forcing increases, the flow continues to accelerate reaching velocities of 0.9 m s^{-1} three hours into the flood tide (transect 24 and 1). Downstream of the crest, a two-layer structure emerges where the current is considerably weaker, around 0.3 m s^{-1} , above the 23.0 kg m^{-3} isopycnals compared to the current underneath.

Meanwhile, in the down-fjord basin, a stagnant region has persisted for more than 3 hours into the flood tide even when water above and below was moving toward the crest. On figure 10, which shows the three-dimensional averaged velocity fields for that tide period (transects 1, 2, 41, 42 and 21 to 24) we see that the stagnant region is also present in the vertical and across-transect component of the flow. As the stagnant region starts moving (transect 25 and 3), the 23.6 kg m^{-3} isopycnal rises 10 m above the crest in the down-fjord basin.

About four hours after the low tide (transects 25-26 and 2), the main flow begins to move down forming a downslope flow above the up-fjord face of the sill. The downslope flow reaches its peak intensity in the following hours (transects 26 and 3-4). At peak intensity, the downslope flow is up to 80 m thick and reaches velocity of 1 m s^{-1} 2000 m past the

crest. Upstream of the crest, the 22.25 kg m^{-3} isopycnal, together with the pycnocline lower boundary, are both less than 10 m below the pycnocline center. Above the crest, the pycnocline lower boundary deepens, sinking more than 10 m below the pycnocline, and moves back up further downstream. However, the 22.25 kg m^{-3} isopycnal remains nearly 30 m below the pycnocline downstream of the crest. In the last hour of the flood tide (transect 27-28 and 5-6), the flow begins to relax and the deep isopycnals move back to their average depths. The acoustic image of transect 28, figure 11a, reveals that as the flood tide flow relaxes, large instabilities are generated between depths of 40 and 80 m in the up-fjord basin. These instabilities form around a small density step ($\sim 1 \text{ kg m}^{-3}$).

Reaching high tide (transects 29 and 7-8), the flood tide flow has not completely relaxed and currents up to 0.6 m s^{-1} persist over the sill. The flow relaxes in two regions across the sill; in the up-fjord basin above depth of 40 m and in the down-fjord basin below depth of 40 m. One hour after high tide (transects 30-31 and 9), the remaining up-fjord currents have vanished and water above the sill crest begins to flow down-fjord. Shortly after, less than 2 hours after high tide (transect 10), the flow above the crest accelerates to 0.7 m s^{-1} . The flow then begins to move down the sill slope below the 22.25 kg m^{-3} isopycnal which has deepened to depth of 35 m at the crest. Meanwhile, deep isopycnals have started to rise above their average depth in the up-fjord basin. Two hours after high tide (transect 11, 32-33), a downslope flow forms above the down-fjord face of the sill. The acoustic image of transect 32, figure 11c, suggests that the upper boundary of the downslope flow is marked by shear-induced instabilities. Furthermore, figure 11c also shows that the downslope flow lies mostly below the region sampled by the ADCP. From the velocities measured above the crest and at the upper limits of the downslope flow, we can speculate that currents within the downslope flow are likely over 0.8 m s^{-1} .

In the second half of the ebb tide (transect 11, 32), what looks like an internal hydraulic jump appears to form between 1400 and 1600 m pass the sill crest. The acoustic image and the velocity vectors of transect 32, figure 11c, show that the internal hydraulic jump begins

to build up around the third hour of the ebb tide. In the following hour (transect 13-14, 34), the downslope flow reaches its peak intensity and the internal hydraulic jump grows to an approximate height of 90 m. The internal hydraulic jump structure is presented in details in figure 11b which shows the acoustic image and the along-transect and vertical components of the flow for transect 14 over the down-fjord half of the sill. The averaged three-dimensional velocity field of transects 13, 14 and 34, figure 12, reveals that both the downslope flow and the internal hydraulic jump have important cross-fjord flow component (west) with velocities up to 0.5 m s^{-1} . This can be explained by the fact that the isobaths of the down-fjord slope of sill B are not perpendicular to the transect line but rather intersect at an approximate angle of 30 degrees (figure 5). The weakly stratified layer also has a small, between 0 and 0.2 m s^{-1} , but coherent cross-fjord flow component in the opposite direction (east). Four hours after high tide (transect 35-36-37 and 15-16-17), the amplitude of the internal hydraulic jump starts to decrease as the tidal forcing slackens. The internal hydraulic jump ultimately dies out within an hour of the low tide (transect 18 and 38) leaving only a down-fjord flow with velocities up to 0.5 m s^{-1} above the sill crest.

1.4.2 Sill B internal hydraulic jump and internal waves

Similarly to what is described in Farmer and Armi (1999b), the internal hydraulic jump is preceded by the formation of a weakly stratified layer that begins to form approximately one hour after high tide (transects 31 and 9-10). After an initial deepening of the near surface stratification, shear-induced instabilities form above the main flow forming the entrainment interface of the weakly stratified layer. The instabilities of entrainment interface are visible on the acoustic images of transect 32 (figure 11c). Throughout most of the second half of the ebb tide, the density structure is as follows: upstream of the crest ($\sim 1500 \text{ m}$), the pycnocline lower boundary together with the 22.25 and 23.0 kg m^{-3} isopycnals are all above the depth of 30 m. Passed the sill crest, these isopycnals slope down along the entrainment interface before they, one-by-one, detach from the entrainment interface and rise quickly above the

internal hydraulic jump.

The same density structure was observed over the down-fjord side of sill B during the winter survey (figure 13) which shows the density field for the fourth hour of the ebb tide. The density field was obtained by horizontally and linearly interpolating reordered density measurements. Red dots are placed along the CTD tracks where density overturns occurred in the density profiles. Following the method proposed by [Galbraith and Kelley \(1996\)](#), any inversions composed of less than 5 consecutive measurements were disregarded as noise and not as real density overturns.

In winter conditions, the pycnocline center and its lower boundary are located around the same depths as in the summer experiment (figure 6) but with higher density values of $\sigma_t = 18.5 \text{ kg m}^{-3}$ and $\sigma_t = 22.2 \text{ kg m}^{-3}$ respectively. Using the same reference depths as for the summer experiments, we have selected densities of $\sigma_t = 23.2$ ($d = 20 \text{ m}$), 23.8 ($d = 40 \text{ m}$) and 24.15 kg m^{-3} ($d = 80 \text{ m}$). The maximum vertical excursion of the reference isopycnals, with the exclusion of the pycnocline center which maintains a relatively constant depth, are approximately 7, 15, 30, and 45 meters below their average depths, in order of increasing densities. Although no velocity measurement are available, the density structure shows clear evidence of a weakly stratified layer that starts approximately 400 m from the sill crest ($d \sim 10 \text{ m}$) to 1700 m at maximal depth ($d \sim 100 \text{ m}$) ending 300 m further down-fjord. The location and extent of the weakly stratified layer places the internal hydraulic jump at about 1800 m from the sill crest with an estimate height of 110 m above the bottom. Furthermore, the presence of density inversion within the weakly stratified layer and around the internal hydraulic jump suggests that the internal hydraulic jump is breaking.

Wave patterns in the acoustic images and horizontal shear in the vertical velocities of transect 34, 36 and 37 (figures 14) suggest that internal waves are propagating upstream of the crest during the ebb tide. The internal waves are centered at depths of 10 m to 20 m and have maximal amplitude of $\sim 15 \text{ m}$.

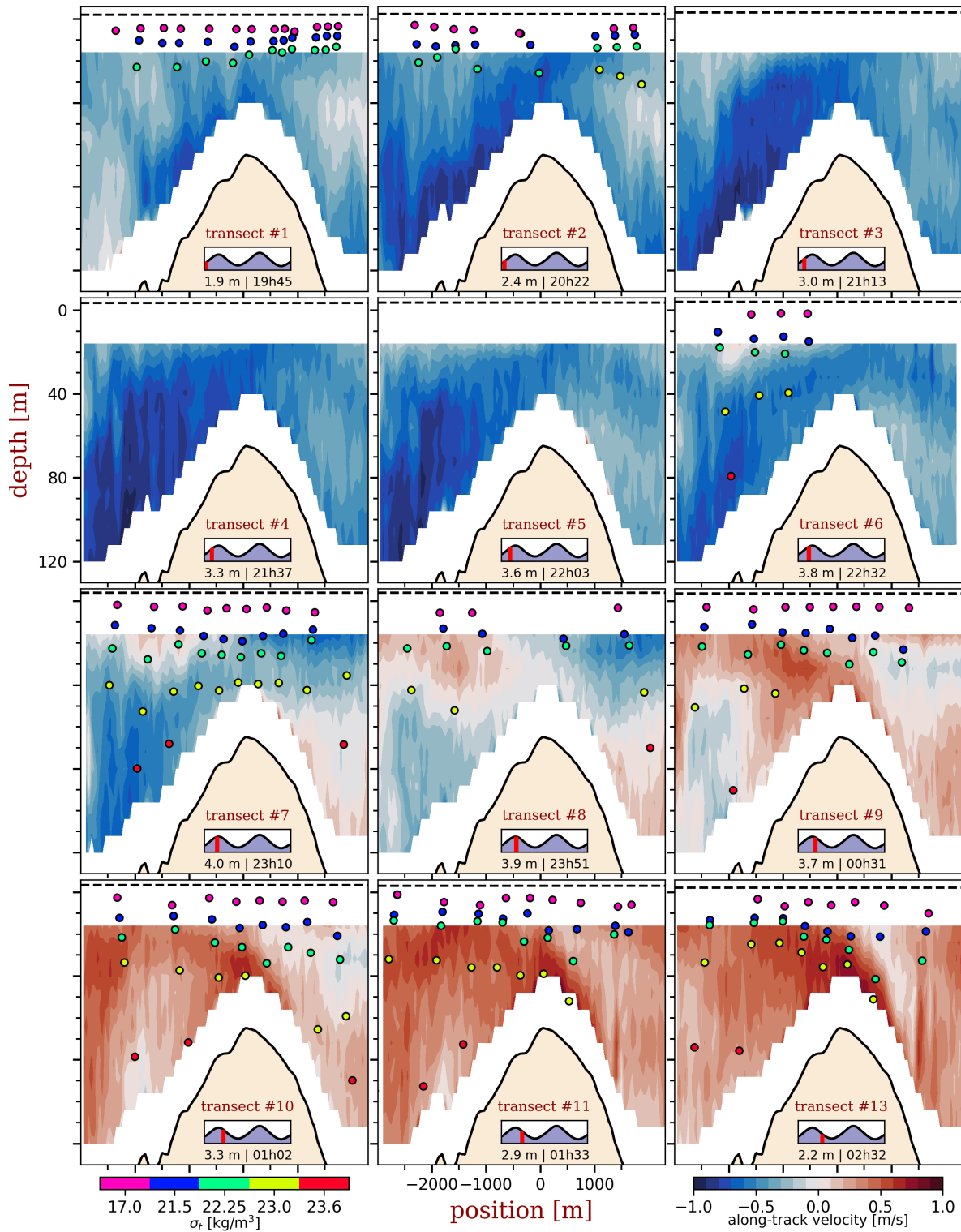


Figure 8 (a): Complete sequence of transects over sill B showing the along-track component of the flow and the density measurements. The horizontal dotted line corresponds to the surface level. Insets show the transect number, a tide gauge with the transect time-span in red, the average surface level and the time of each transect. (a) Density measurements are missing below depth of 50 m on transects 1 and 2, up-fjord of the crest on transect 6 and none are available on transects 3,4 and 5.

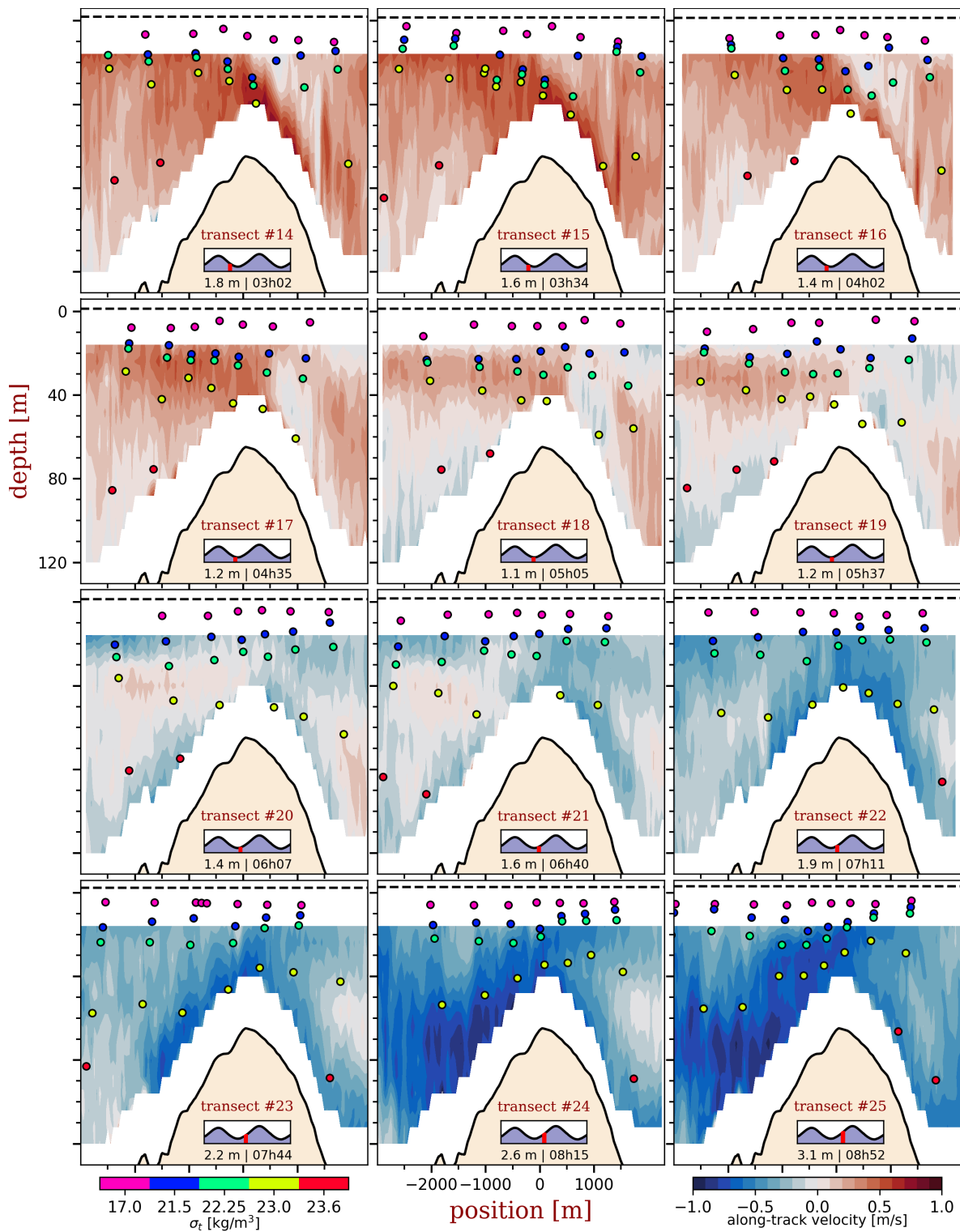


Figure 8 (b): (Cont)

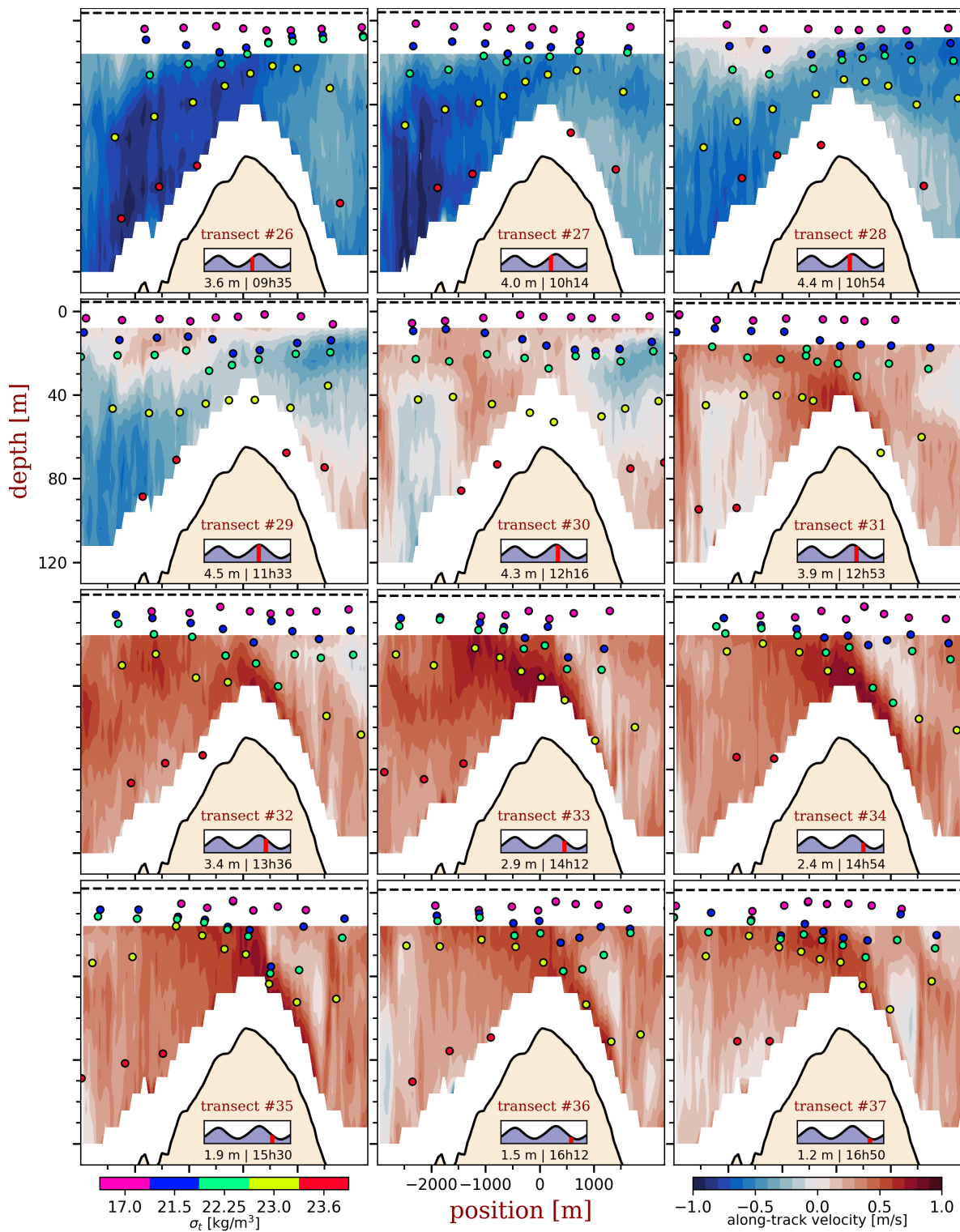


Figure 8 (c): (Cont)

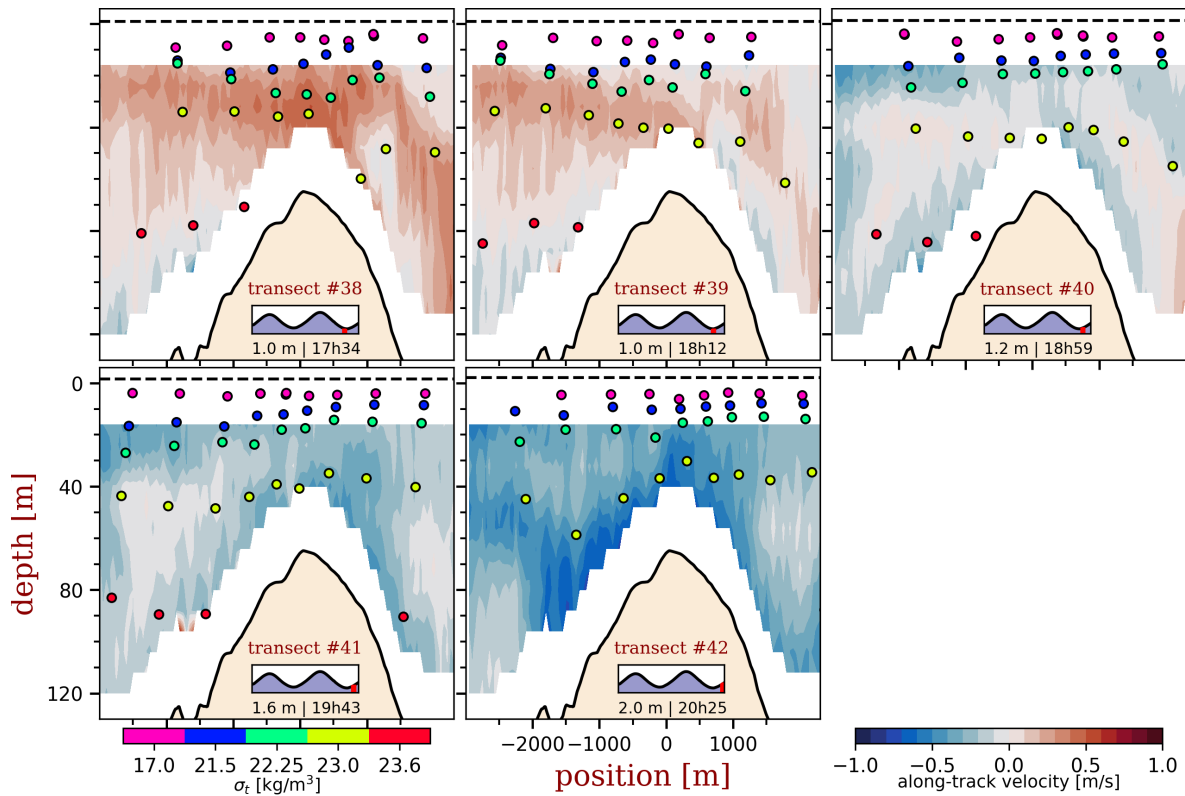


Figure 8 (d): (Cont)

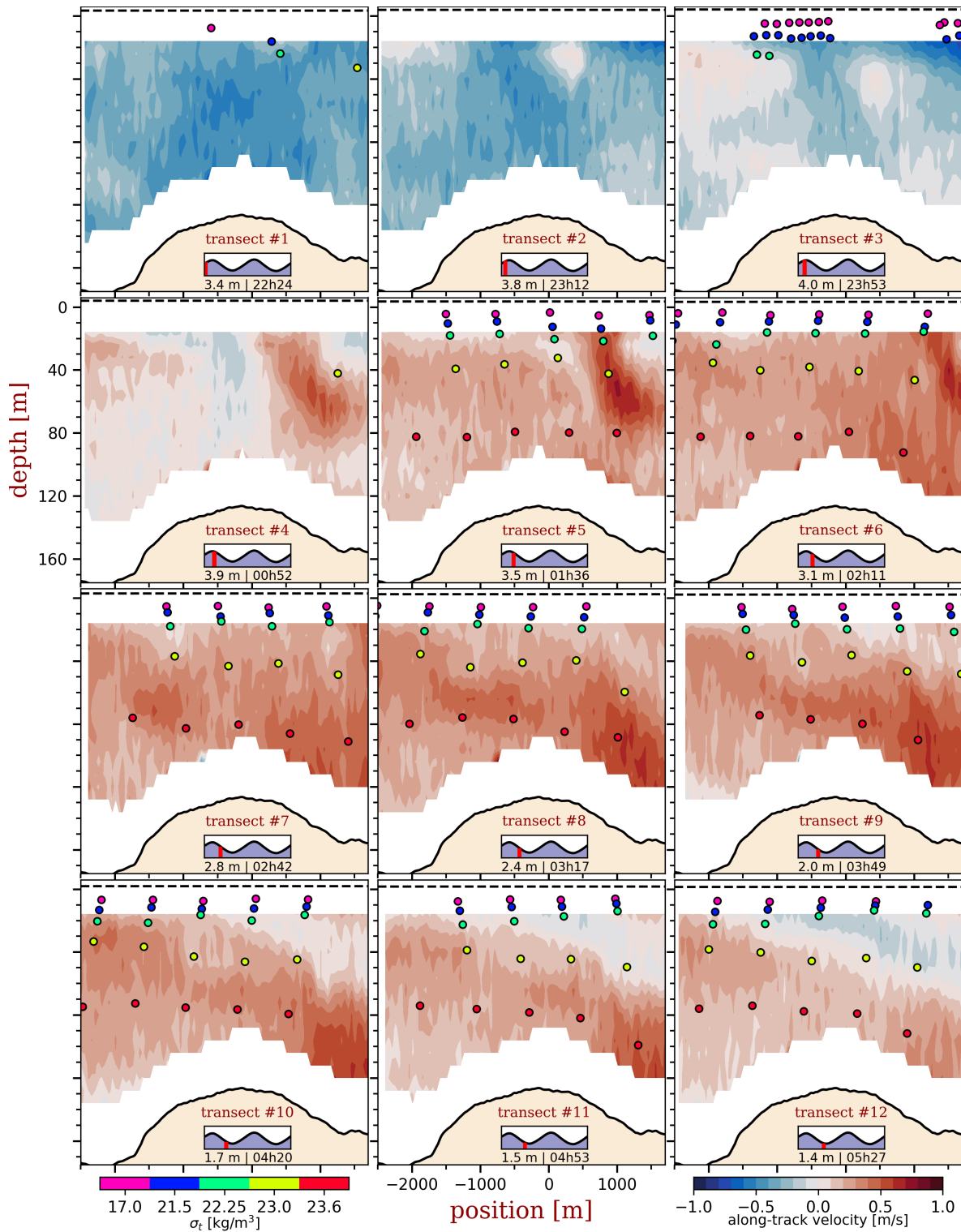


Figure 9 (a): Complete sequence of transects over sill C showing the along-track component of the flow and the density measurements. The horizontal dotted line corresponds to the surface level. Insets show the transect number, a tide gauge with the transect time-span in red, the average surface level and the time of each transect.

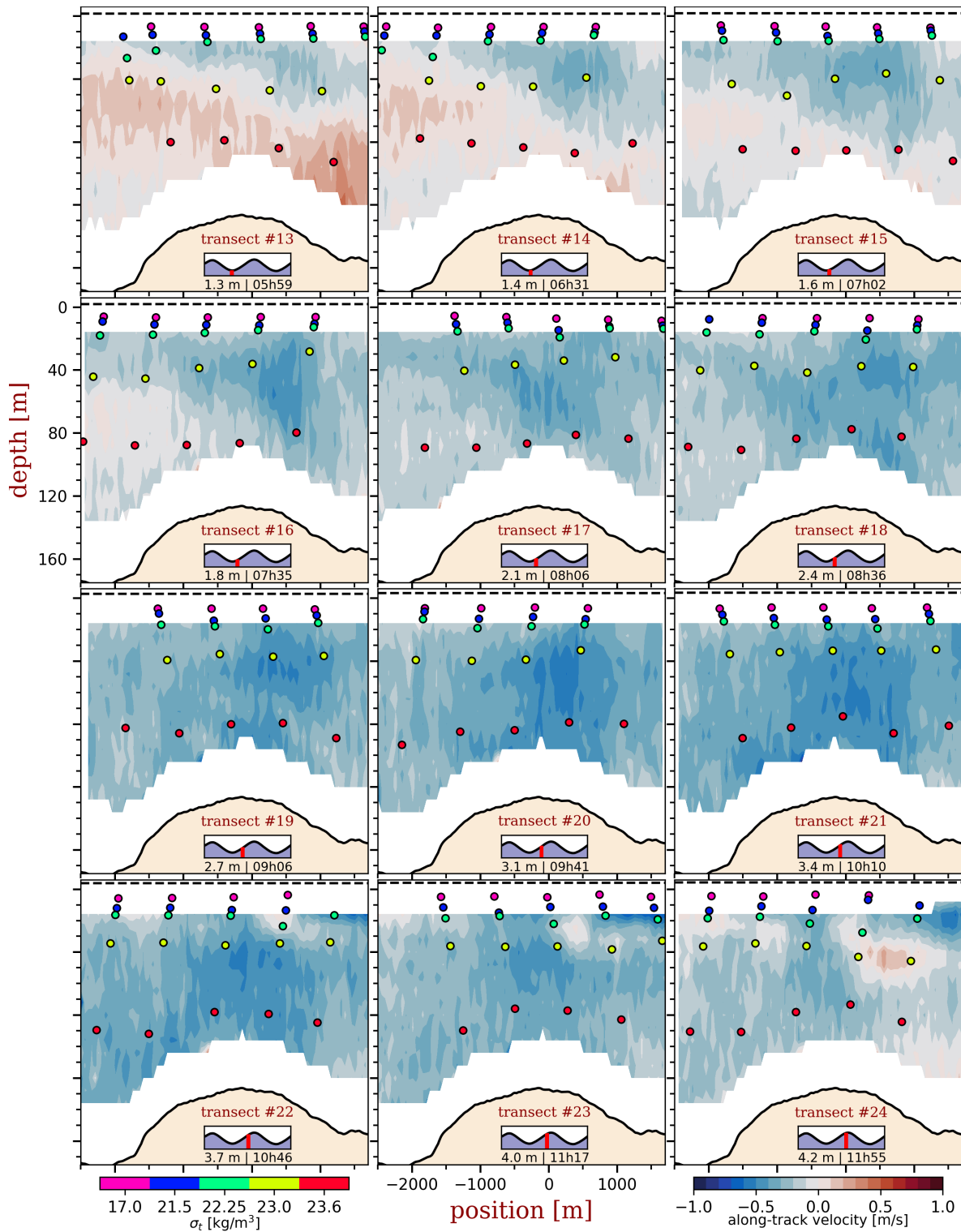


Figure 9 (b): (Cont)

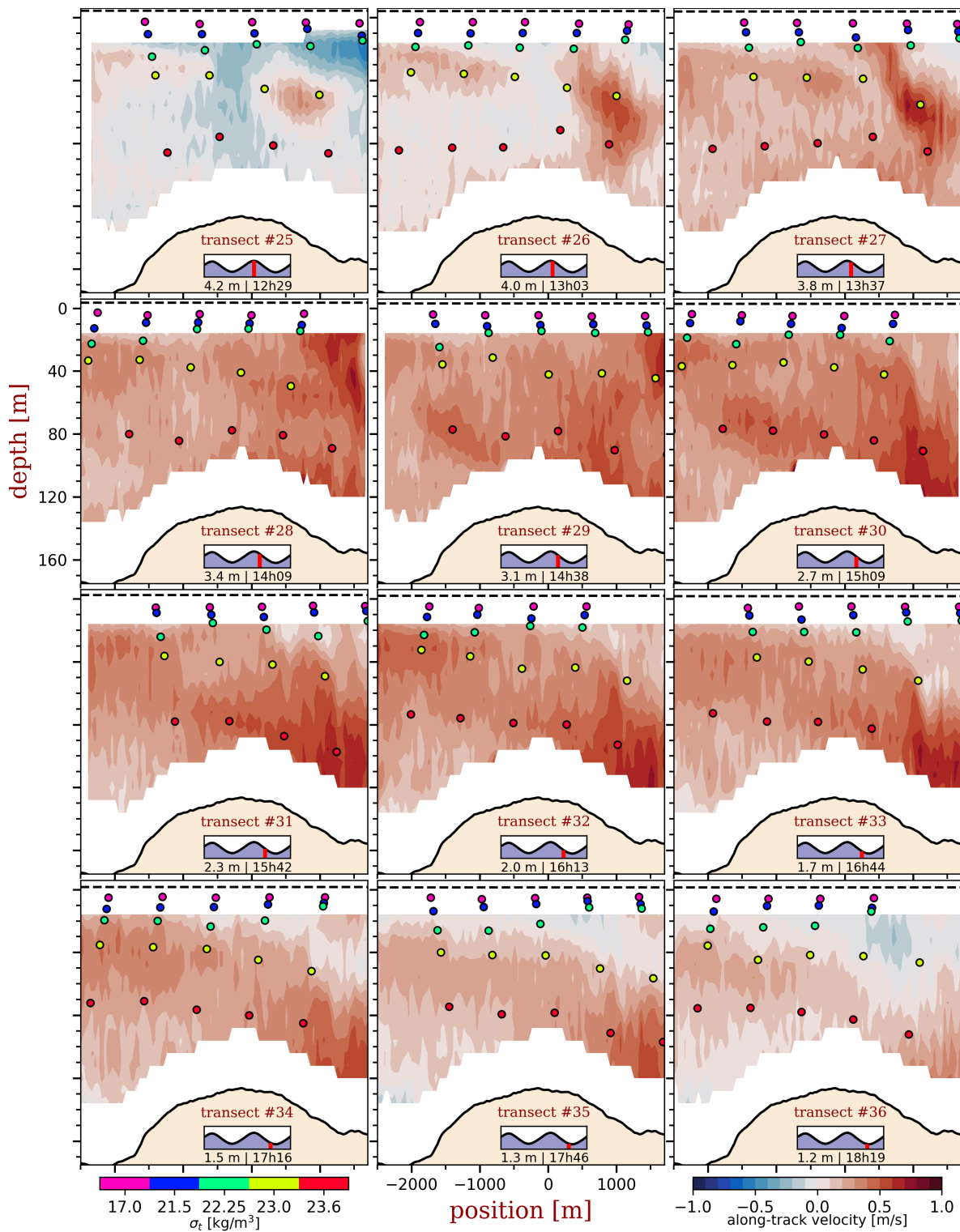


Figure 9 (c): (Cont)

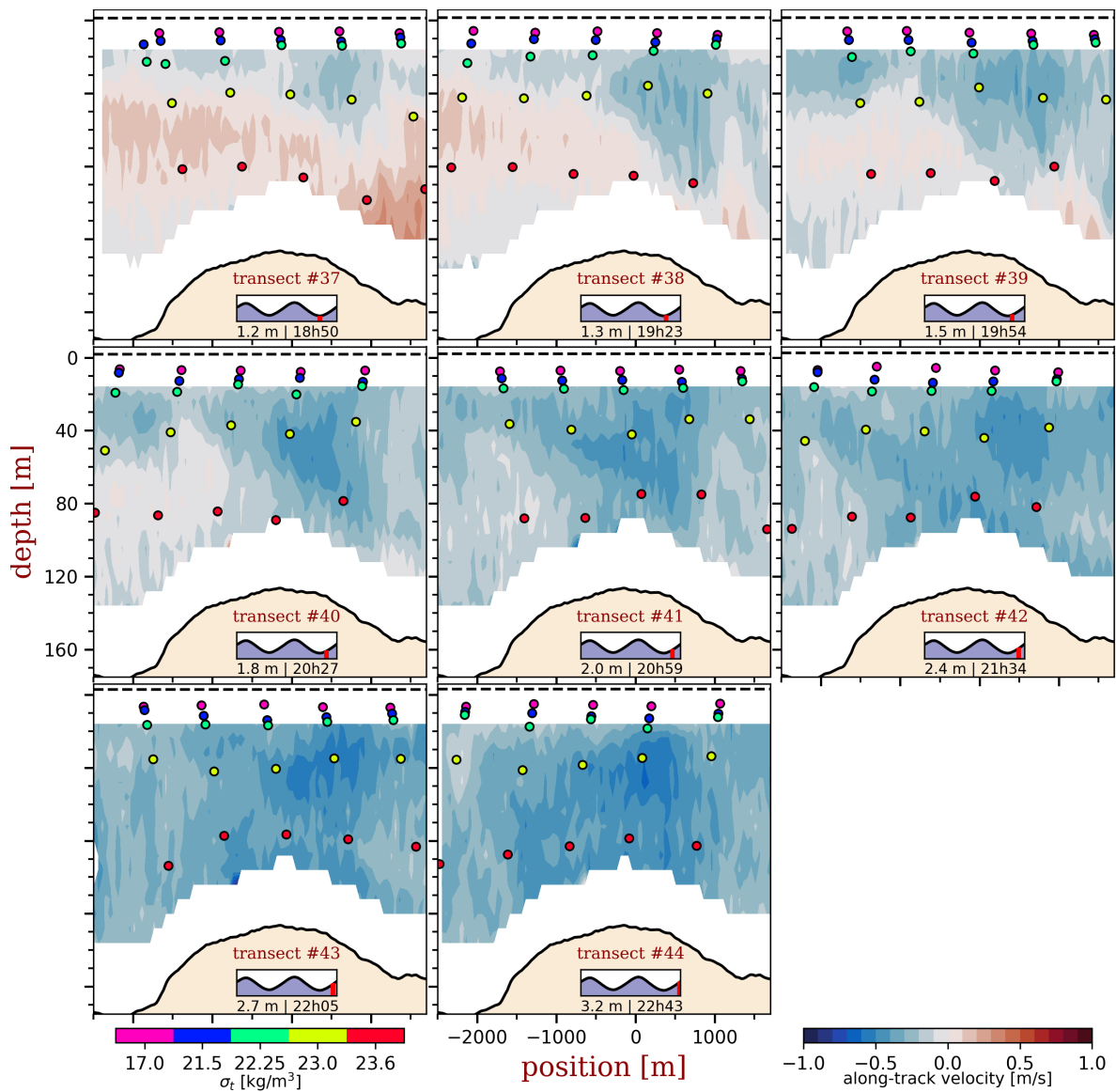


Figure 9 (d): (Cont)

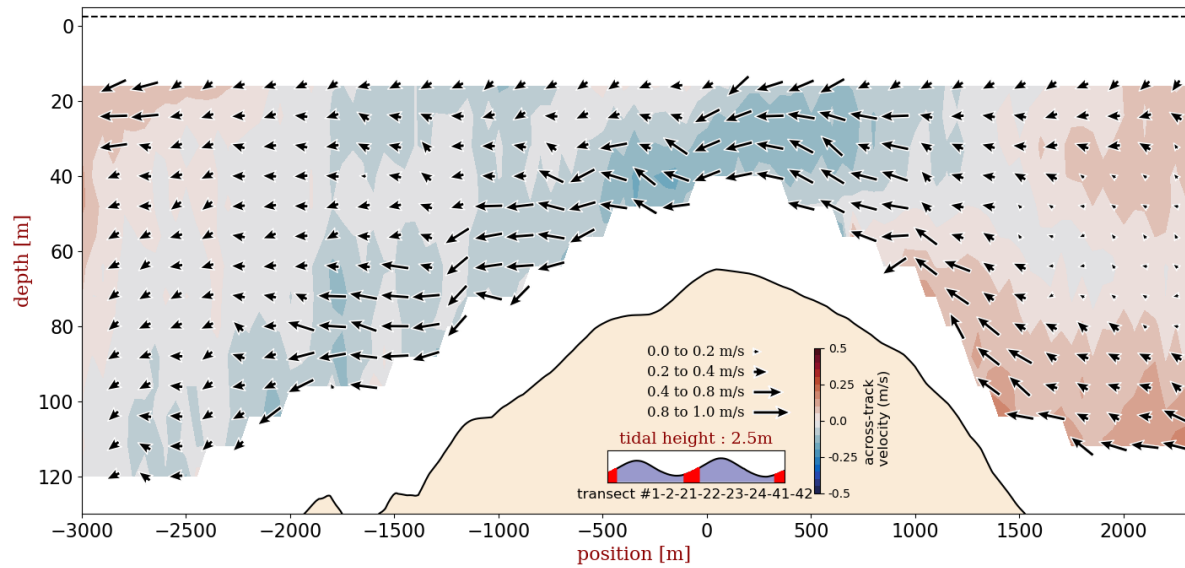


Figure 10: Along and across transect components of the flow velocity averaged over the transects 1, 2, 21, 22, 23, 24, 41 and 42. Positive across-track velocities are outgoing.

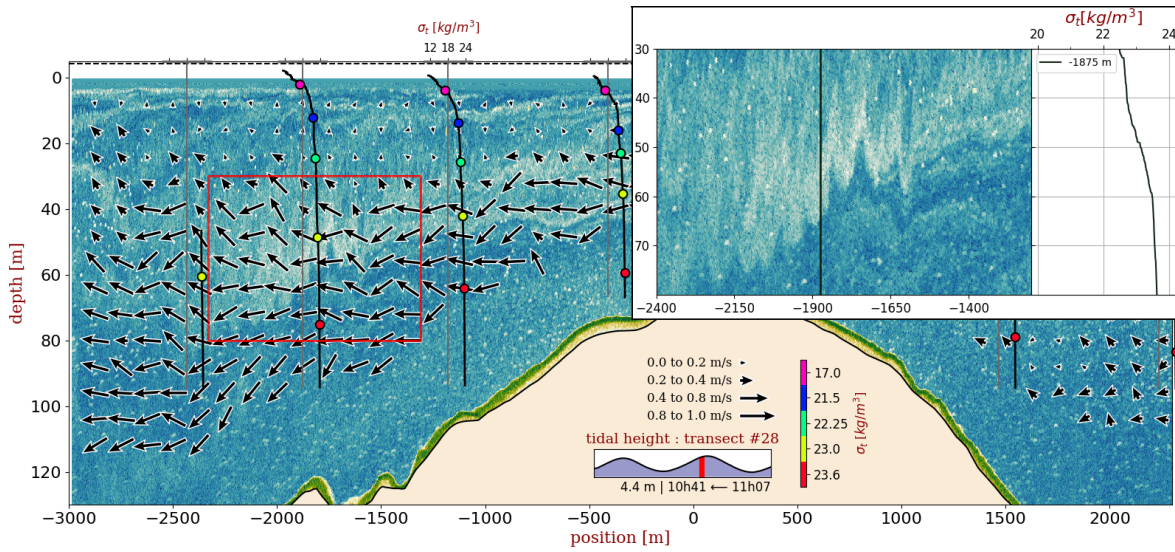
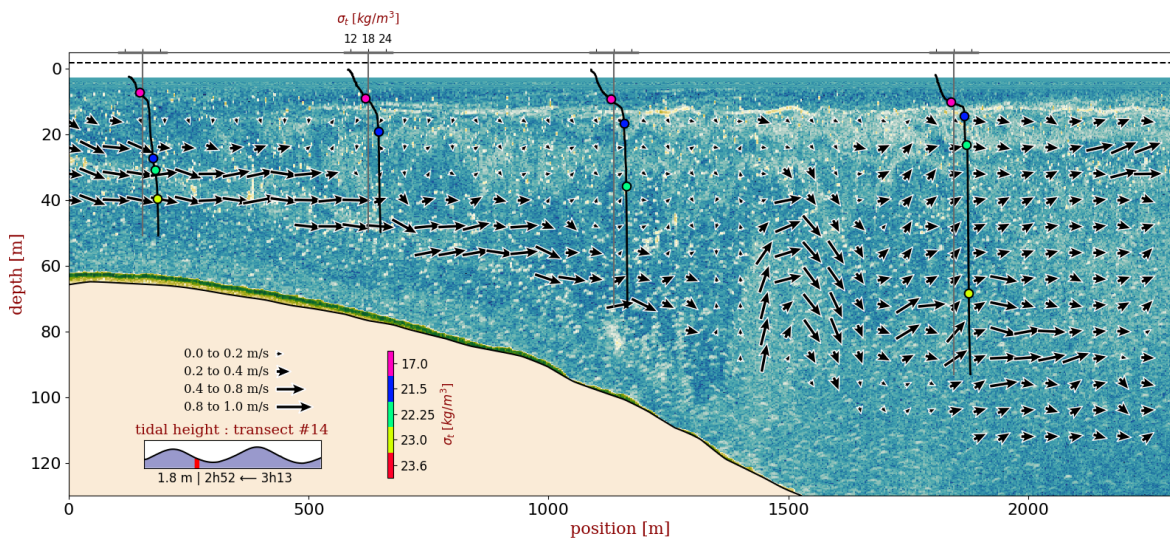
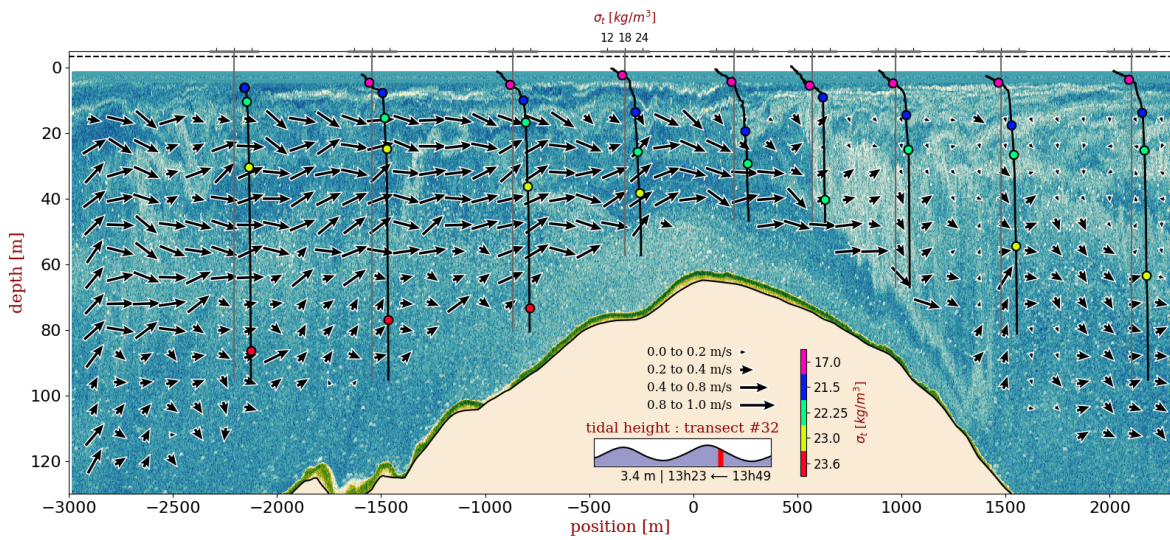


Figure 11 (a): Transect over Sill B showing the acoustic image (arbitrary units) with a color scale ranging from blue to white to green, with green representing stronger backscatter, along-transect and vertical components of the flow with vectors grouped in bins of 0 to 0.2, 0.2 to 0.4, 0.4 to 0.8 and 0.8 to 1.0 m/s and density profiles. Note that the angle of the vectors follows the vertical to horizontal aspect ratio which exaggerates the contribution of the vertical component of the flow and that the horizontal position of the highlighted density measurements doesn't correspond to their actual location. Insets show the transect number, a tide gauge with the transect time-span in red, the average surface level, the time and an arrow that indicates the direction of travel. (a) The red box correspond to the close-up shown in the top right inset. The black vertical line in the close-up indicates the location of the density profile also shown in the inset. The horizontal dotted line corresponds to the surface level. (b) Close-up of the down-fjord half of sill B. The horizontal dotted line corresponds to the surface level.



(b)



(c)

Figure 11: (Cont)

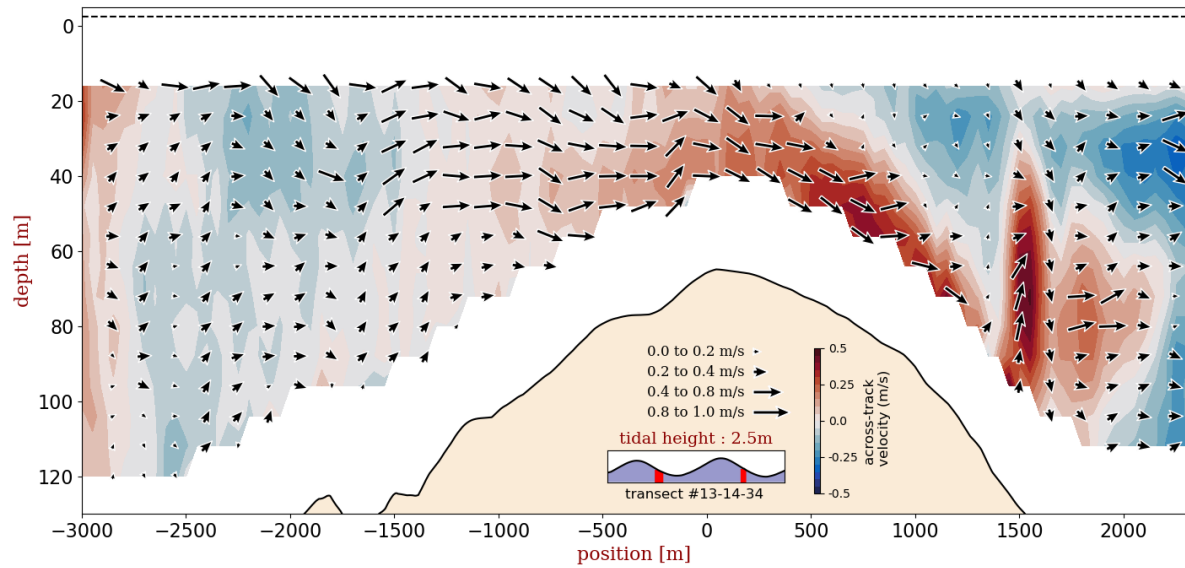


Figure 12: Along and across transect components of the flow velocity averaged over the transects 13, 14 and 34. Positive across-track velocities are outgoing.

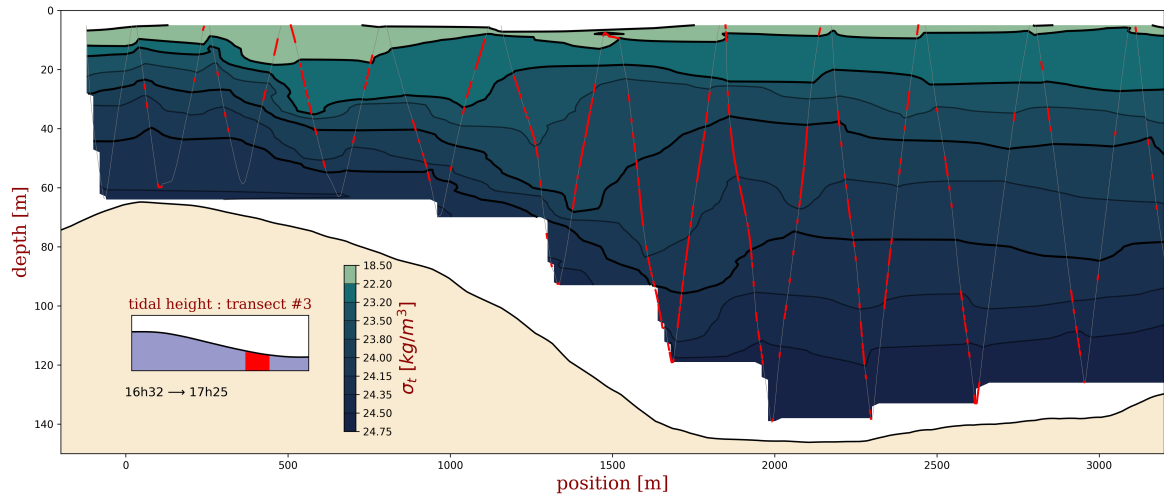


Figure 13: Horizontally interpolated density field of the third transect of the 2020 winter survey on March 2nd 2020. The thick black lines correspond to the winter reference isopycnals that of densities of $\sigma_t = 18.5, 22.2, 23.8$ and 24.15 kg m^{-3} . The high tide was 4.2 m at 12h15 and low tide was 1.44 m at 18h30 measured at Port-Alfred, La Baie, 100 km from the mouth. The light grey line shows the track of the CTD probe and the red dots show density inversions.

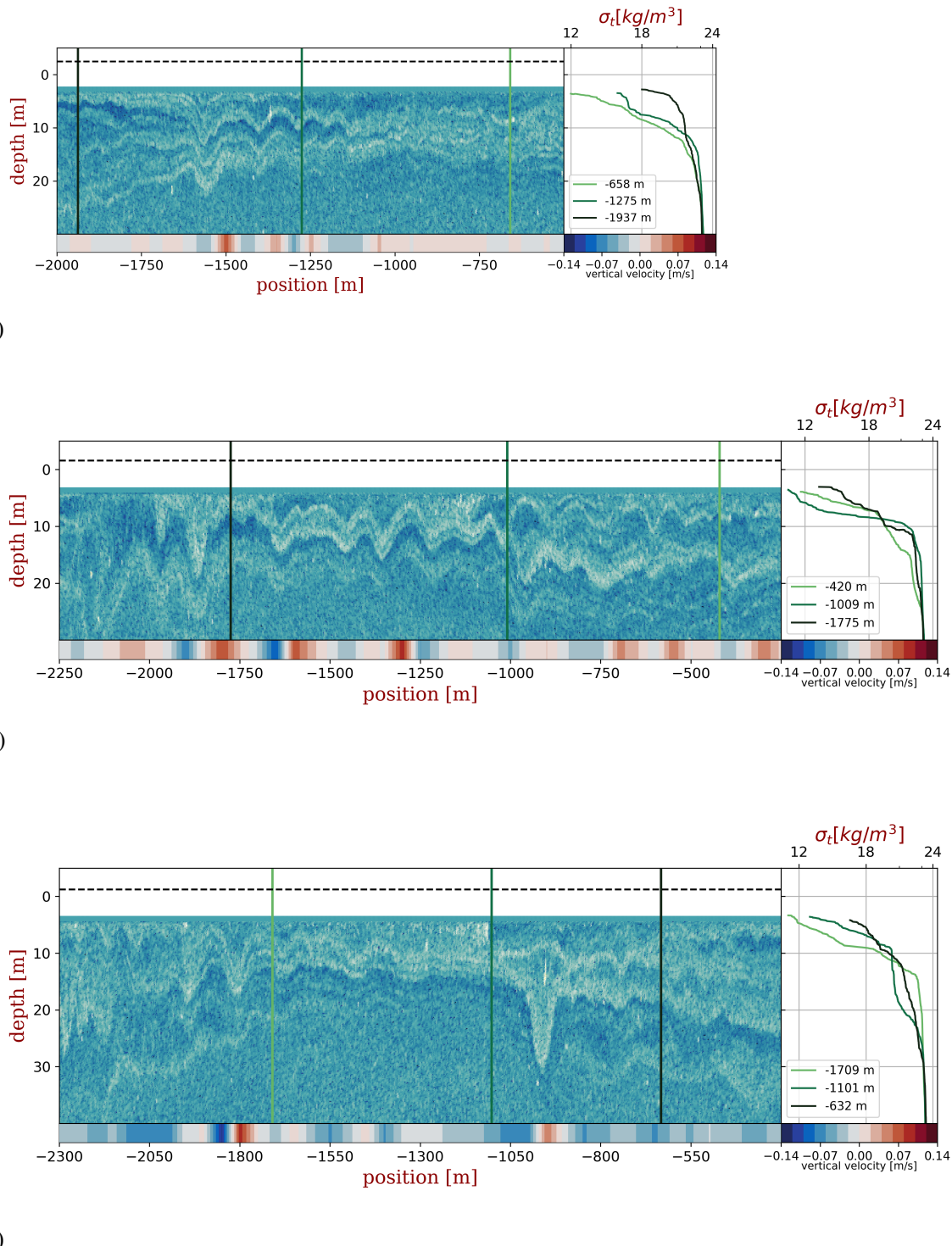


Figure 14: Transect Sill B showing the acoustic image (arbitrary units) with a color scale ranging from blue to white, with white representing stronger backscatter. The vertical lines indicate the location of the density profiles of the corresponding color. The average vertical velocity fields are shown under the acoustic images with a red to blue color scale. (a) Transect 34. The vertical velocities were averaged over the first 20 m. (b) Transect 36. The vertical velocities were averaged over the first 30 m. (c) Transect 37. The vertical velocities were averaged over the first 30 m.

1.4.3 Flow across sill C

In the 2 hours preceding the low tide which correspond to the transects 10-12 and 32-36 in figure 9, both the 23.0 kg m^{-3} and 23.6 kg m^{-3} isopycnals slope down into the down-fjord basins whilst the 22.25 kg m^{-3} isopycnal begins to slope up. The widening of the layer formed by the 22.25 kg m^{-3} and 23.0 kg m^{-3} isopycnals coincides with the appearance of an up-fjord current around the same location. This suggests that as the barotropic forcing weakens, buoyancy forces pushes water upstream above the main down-fjord tidal flow that slopes down into the down-fjord basin. At low tide, i.e. transects 13 and 37, the down-fjord and up-fjord currents are approximately equal in strength with water velocities around 0.2 to 0.3 m s^{-1} . In the hour following the low tide, the remaining ebb tide current decreases and down-fjord of the crest the 23.0 and 23.6 kg m^{-3} isopycnals move up to their averaged depth. On the acoustic images of transects 11 to 14 (figure 15) we see that the interface between the down-fjord and up-fjord currents is marked by shear-induced instabilities.

In the first half of the flood tide (transects 14-19 and 38-42), the barotropic forcing increases thus accelerating water up-fjord. As it moves over the sill, the water is further accelerated but slows back down once it reaches the up-fjord basin. The tidal flow reaches maximum intensity about 4 hours after the low tide (transect 20 and 43-44). At peak intensity, the strongest currents are found above the crest at 0.6 m s^{-1} between depths of 30 m and 80 m. Again, stronger currents could lie within the blank regions near the sill face. Furthermore, the pycnocline lower boundary and the 22.25 kg m^{-3} isopycnal deepen slightly above the sill crest. In the second half of the flood tide (transects 21-23 and 1-2), the intensity of the flow decreases. However, just below the pycnocline, water upstream of the crest accelerates up-fjord to velocities up to 0.6 m s^{-1} .

Reaching the high tide (transects 3 and 24), a small pocket of water located slightly down-fjord of the crest, between depths of 30 m and 60 m, begins to move down-fjord while the water above still flows up-fjord at about 0.4 m s^{-1} . These opposite currents lead to shear-

induced instabilities that can be seen on the acoustic images of the transects 24 and 25 (figure 16). During the first hours after the high tide (transects 25-26 and 4), the remaining flood tide currents decrease and the ebb tide current gains in strength, especially in the down-fjord basin where, at depths ranging from 20 to 80 m, water quickly accelerates down-fjord to velocities up to 0.6 m s^{-1} . Furthermore, the acoustic images of transects 26 (figure 16) shows that this rapid down-fjord acceleration generates further instabilities in the down-fjord basin. In the hour that follows, (transects 27-28 and 5-6, figure 9), the initial maximum core of the ebb flow moves downstream of the crest as the current within it reaches $\sim 0.7 \text{ m s}^{-1}$.

In the hour before mid ebb tide (transects 29 and 7), water starts to accelerate down the down-fjord face of the sill forming a 60 meter thick downslope flow. Simultaneously, the 23.0 kg m^{-3} and 23.6 kg m^{-3} isopycnals begin to slope down towards the down-fjord basin. At peak tidal forcing (transects 30-33 and 8-9), the downslope flow reaches velocities of $0.7\text{-}0.8 \text{ m s}^{-1}$ about 1250 m from the crest. The 23.0 kg m^{-3} and 23.6 kg m^{-3} isopycnals are both about 10 m above their average depth upstream of the crest and about 10 m below downstream. When fully established, the main flow extends upstream of the crest rising above depths of 80 m with an upper limit around depths of 20 m.

Two hours before the low tide (transects 33-35 and 10-11), the 22.25 kg m^{-3} isopycnal rises by about 10 m downstream of the crest while remaining at a depth of 20 m upstream. Thus in the down-fjord basin, the layer between the 22.25 and 23.0 kg m^{-3} isopycnals widens by about 20 m in the second half of the ebb tide. Consequently, current within this layer is about $0.3\text{-}0.4 \text{ m s}^{-1}$ weaker in comparison to the downslope current below and even begins to reverse moments before the slack tide. Similarly, the currents below the main flow in the up-fjord basin are weaker than in the main flow above and begin to reverse before the end of the ebb tide.

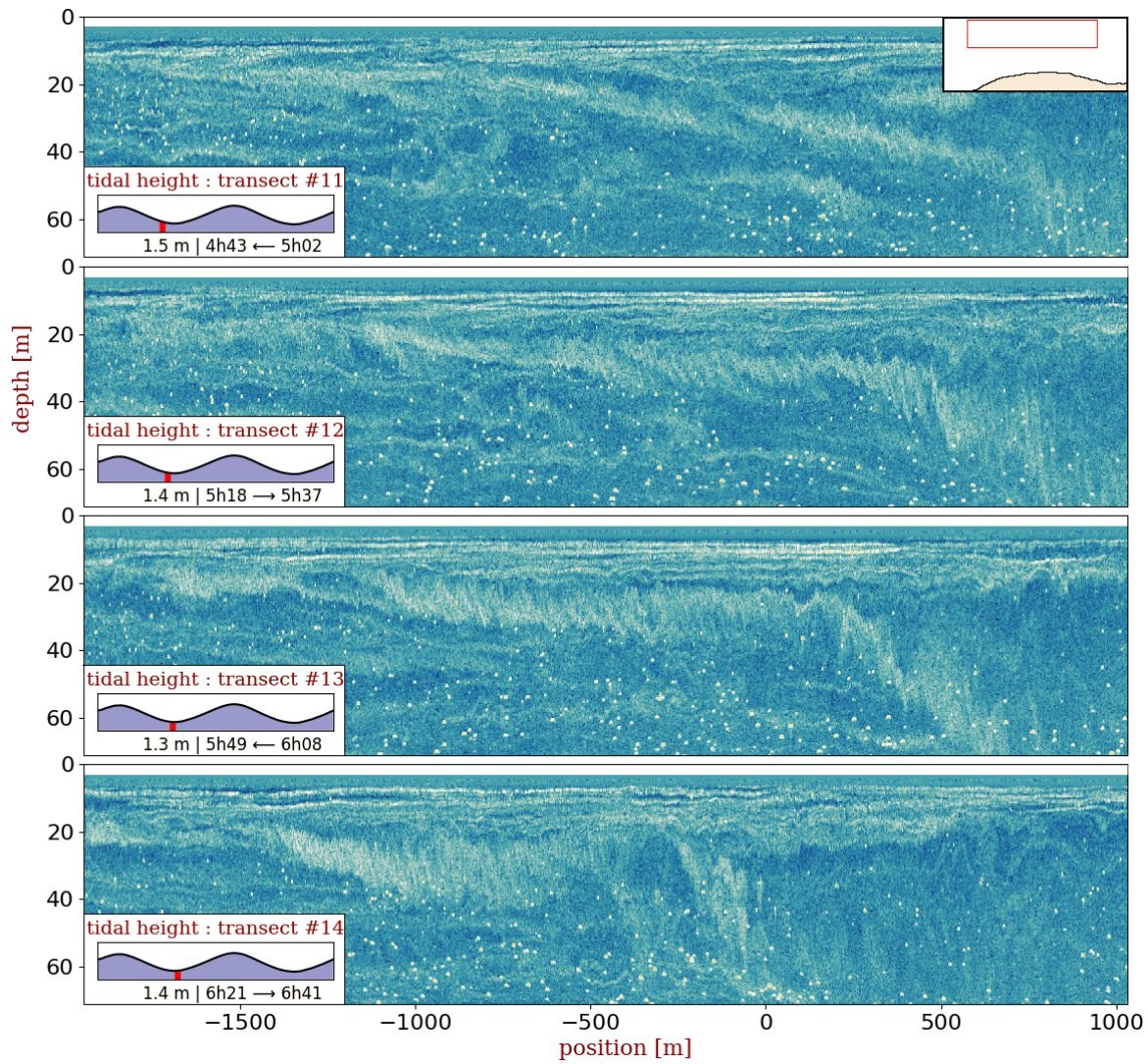


Figure 15: Sequences of transects over sill C showing the acoustic image (arbitrary units) with a color scale ranging from blue to white, with white representing stronger backscatter. Insets on the left show the transect number, a tide gauge with the transect time-span in red, the average surface level, the time and an arrow that indicates the direction of travel. On the top-right corner of transect 11, an inset shows the zoomed-in region in red relative to sill C.

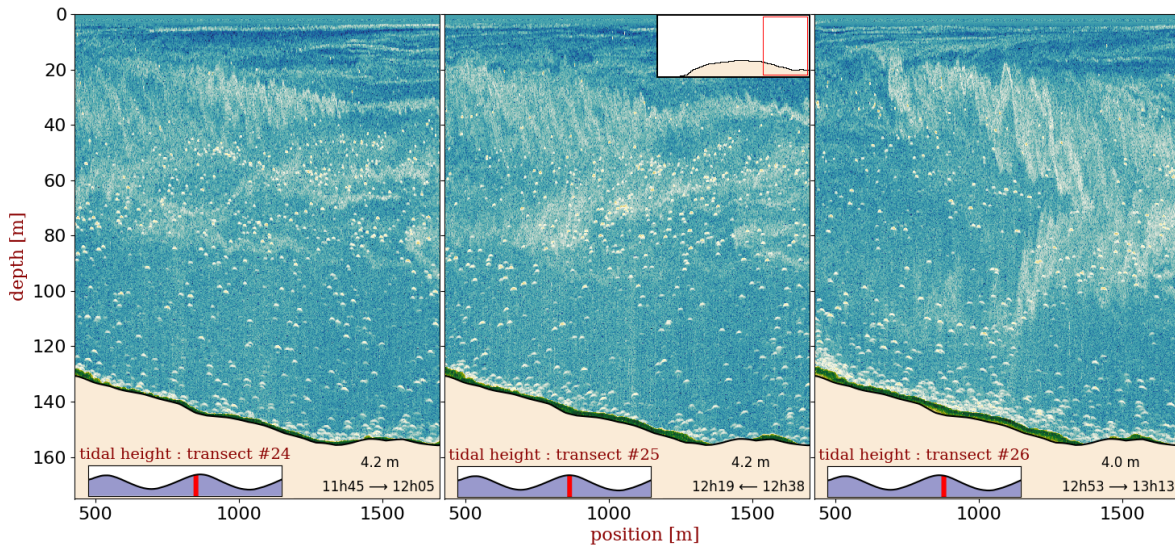


Figure 16: Sequences of transects over sill C showing the acoustic image (arbitrary units) with a color scale ranging from blue to white to green, with green representing stronger backscatter. Insets on the left show the transect number, a tide gauge with the transect time-span in red, the average surface level, the time and an arrow that indicates the direction of travel. On the top-right corner of transect 25, an inset shows the zoomed in region in red relative to sill C.

1.4.4 July 2018 water renewal regime

At first glance, the longitudinal temperature field of the fjord, shown in figure 17, suggests that renewal of the Saguenay Fjord intermediate water is ongoing at the time of the 2018 summer survey. That is, the renewal of the inner basin intermediate water (mid depth) by intruding mixed water at the mouth. A cold subsurface pocket of water ($0.3^{\circ}\text{C} < T < 1^{\circ}\text{C}$, $10 \text{ m} < d < 110 \text{ m}$) near the head of the fjord and an intruding wedge of warmer water ($1.25^{\circ}\text{C} < T < 2^{\circ}\text{C}$) is the expected structure of a summer renewal of the intermediate water as described in Belzile et al. (2016). Furthermore, isopycnals between $23.0 \text{ kg m}^{-3} < \sigma_t < 23.6 \text{ kg m}^{-3}$ are up to 50 m higher in the intermediate basin compared to the inner basin indicating that a baroclinic flow is moving water from the intermediate to the inner basin. However, isopycnals between $23.0 \text{ kg m}^{-3} < \sigma_t < 23.6 \text{ kg m}^{-3}$ are up to 20 m lower in the

intermediate basin compared to the outer basin which suggests that deep water from the intermediate basin should also flow into the outer basin. Similarly, Stacey and Gratton (2001) have modelled episodes of reverse renewals in the Saguenay Fjord that occur when the density of water at depth decreases faster in the outer basin than in the inner basin resulting in a net bottom flow from the inner to the outer basin.

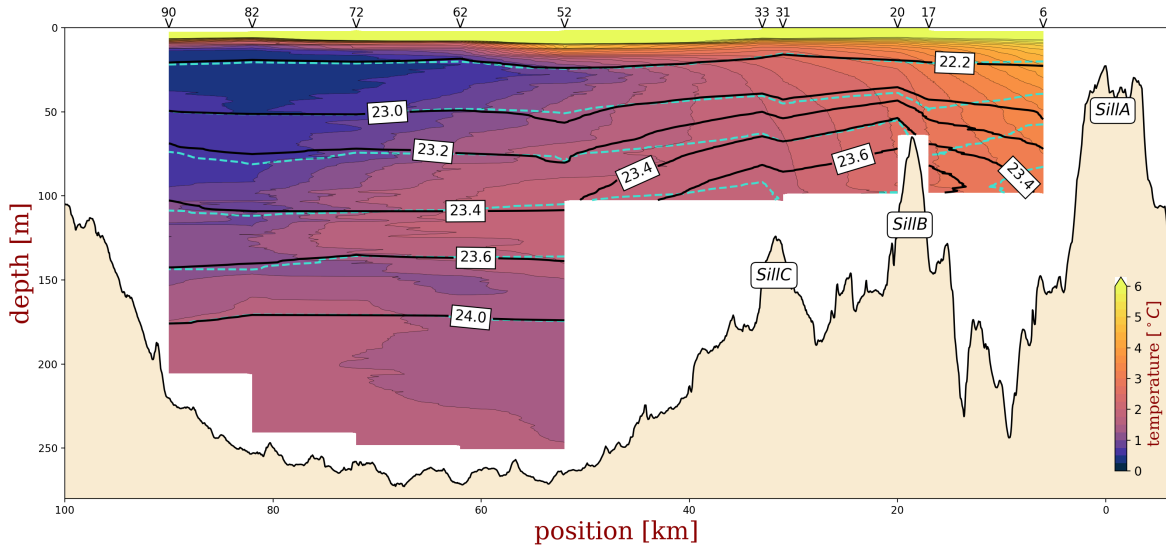


Figure 17: Longitudinal temperature field of the Saguenay Fjord during 3-9 July 2018. The thick black lines and the labels show isopycnals. The cyan dashed lines show isohalines whose depths in the inner basin roughly correspond to those of the selected isopycnals. The longitudinal fields were interpolated from CTD profiles located 6, 17, 20, 31, 33, 52, 62, 72, 82, and 90 km from the mouth of the fjord. The CTD profiles from the sill experiments were averaged into up-fjord profiles (relative position < 0) and down-fjord profiles (relative position > 0) for both sills to remove the semi-diurnal vertical oscillation of the isopycnals resulting in ambient profiles at 17 km, 20 km, 31 km and 33 km. Similarly the profile at 6 km is the average of the 4 CTD casts carried out over 16 hours at that location.

1.5 Interpretation

1.5.1 Upstream and downstream response

The summer observations revealed important upstream and downstream flow responses at sills B and C regarding isopycnal displacement that is rising upstream and sinking downstream of the tidal flow. The isopycnal height differences across both sills are summarized in figure 18. Unsurprisingly, the upstream and downstream responses are greater at sill B due to the shallower depths. Interestingly, when comparing the flood to the ebb tide, we find that the upstream-downstream responses are greater during the ebb tide. Moreover at sill B, the 23.0 kg m^{-3} isopycnal rises 20 m above its average depth during both the flood and the ebb tides but it takes longer (a little more than an hour) to do so during the flood tides. Both the differences in amplitude and the delay in the upstream responses during the flood tides at sill B could be consequences of the presence of denser water up-fjord of the sill.

Similarly to what has been observed by [Klymak and Gregg \(2003\)](#) at the Knight Inlet sill, we see that, for sills B and C, the upstream compression of the mid depth isopycnals, that is approximately between the pycnocline lower boundary and the 23.6 kg m^{-3} isopycnal, leads to an acceleration of the mid depth flow e.g., on transect 11 over sill B ([8a](#)) and on transect 32 over sill C ([9c](#)).

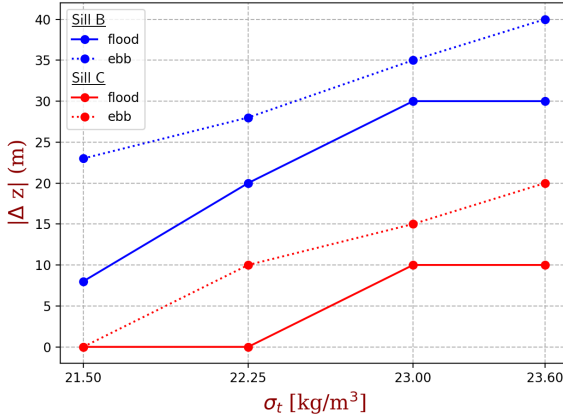


Figure 18: Maximal isopycnals height difference across sills B and C for the ebb and the flood tide.

The flow over the sills B and C never completely relaxes during the slack tides. On one hand, the main tidal current, although weakened, always persists during the slack tides and only decreases in the first hour or so of the following tidal cycle e.g, transect 30 over sill B (figure 8c). On the other hand, part of the water column begins to move slowly ($<0.2 \text{ m s}^{-1}$) opposite of the tidal flow before the reversal of the tidal forcing e.g, transects 11 to 14 over sill C (figures 9a and 9b). Nearing the slack tides, the deeper isopycnals are still higher upstream thus baroclinic forces are present across the sill. As the barotropic forcing becomes weaker than the baroclinic forces, the displaced isopycnals start to move back to their averaged depths. Consequently, the water upstream of the crest that was blocked or partially blocked by the sill and the water above the main flow begins to move opposite to the tidal stream. The water above the main flow thus forms an exchange flow in the hour preceding every slack tide except during the low tide over sill B , e.g. transects 38 and 39 (figure 8d), where the current above the max core of the ebb flow only starts to reverse at the low tide. The exchange flow is particularly strong over sill C at the end of the ebb tide , e.g. transect 14 (figure 9b), growing to depth of 50 m during slack tides. These opposing currents around the slack tides lead to shear-induced instabilities as shown by the acoustic images of the flow (figures 11a and 15).

1.5.2 Internal hydraulic jump at sill B

The main finding of this study is the evidence of the formation of an internal hydraulic jump at sill B. Contrary to what has been observed at Knight Inlet sill ([Farmer and Armi, 1999a](#)) there is no apparent flow separation at the Saguenay Fjord sill B prior to the growth of an internal hydraulic jump. Rather than being pushed down by the expansion of the weakly stratified layer, the flow seems to immediately move down along the sill slope. This could be a consequence of the more gradual slope for the sill (~3,6% for sill B vs ~20% for Knight Inlet sill).

Furthermore there is a flood-ebb tide asymmetry in the flow response where an internal hydraulic jump only forms during the ebb tide. The presence of denser water up-fjord of the crest, as shown in figure 17, seems to hinder the formation of an internal hydraulic jump. Similar to what has been observed at Knight Inlet sill by [Klymak and Gregg \(2003\)](#), the tidal flow initially detaches from the sill face due to the presence of denser water up-fjord of the crest. This density-forced separation ([Klymak and Gregg, 2003](#)) limits the acceleration of the downslope flow, until the denser water, salty pool is flushed further downstream allowing the downslope flow to move deeper and gain more kinetic energy. Since the denser water at sill B is only flushed around mid flood tide, the downslope flow starts loosing its intensity before an internal hydraulic jump can form.

[Farmer and Armi \(1999a\)](#) showed that instabilities at the entrainment interface of the weakly stratified layer can move up the interface and propagate as internal waves upstream of the sill at the pycnocline. Similarly, the combined acoustic images of transects 35 and 36 (figure 19) suggest that large instabilities ($10 \text{ m} < \text{amplitude} < 20 \text{ m}$) generated along the sloping entrainment interface are the source of the internal waves observed during the ebb tide at sill B.

The winter observations (figure 13) revealed important variations in the position and height of the internal hydraulic jump that is 300 m further downstream and 20 m taller

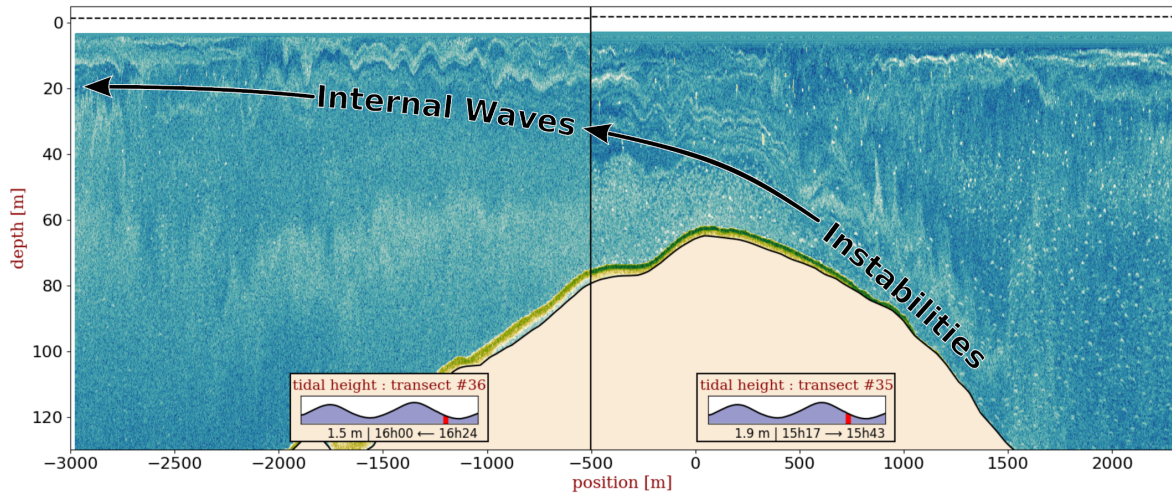


Figure 19: Combined acoustic images of transects 35 (right) and 36 (left) over sill B.

with a thicker weakly stratified layer. Although the internal hydraulic jump was taller in the winter observations, it still stood about 30 m below the surface but started further down the sill slope. Furthermore, the density inversions in the density field suggest that the internal hydraulic jump is breaking and generating turbulent mixing within the weakly stratified layer.

Uncertainties still remain concerning the seasonal variability of the internal hydraulic jump. Seasonal variability in the fjord density structure could play an important role in the formation of internal hydraulic jumps not only on the distance (from the sill crest), the timing, the height or stability but also on which tidal phase it forms (ebb, flood or both). During a deep water renewal regime, denser water is found down-fjord of sill B, thus we could expect to see an internal hydraulic jump during the flood tide.

1.5.3 Lateral constriction of the flow

Looking at the fjord width at sill C, presented in figure 20, we see that the mid depth acceleration of the flow observed in the early moments of the ebb tide coincides with a longi-

tudinal narrowing of the width of the fjord. The longitudinal variation of the cross-sectional area of the fjord at sill C, shown in figure 21, reveals that the location where the fjord is the narrowest, and therefore where the flow is restricted the most, is not at the sill crest but some 750 m further down-fjord. Figure 21 also shows that the depth-integrated along-transect transport, T_{x_t} , defined by

$$T_{x_t}(y) = \sum_z v_{x_t}(y, z) \Delta z, \quad (1.1)$$

peaks near the point of maximum flow restriction. Thus the lateral compression of the flow could be responsible for the unexpected mid-depth flow acceleration.

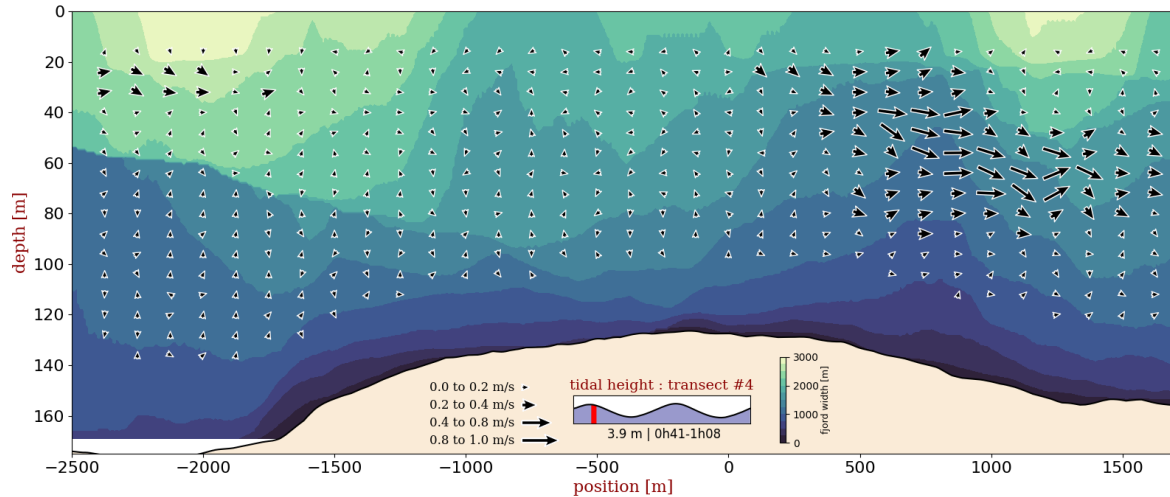


Figure 20: Transect 4 over sill C showing along-transect and vertical components of the flow with vectors grouped in bins of 0 to 0.2, 0.2 to 0.4, 0.4 to 0.8 and 0.8 to 1.0 m/s and the width of the fjord (in colors)

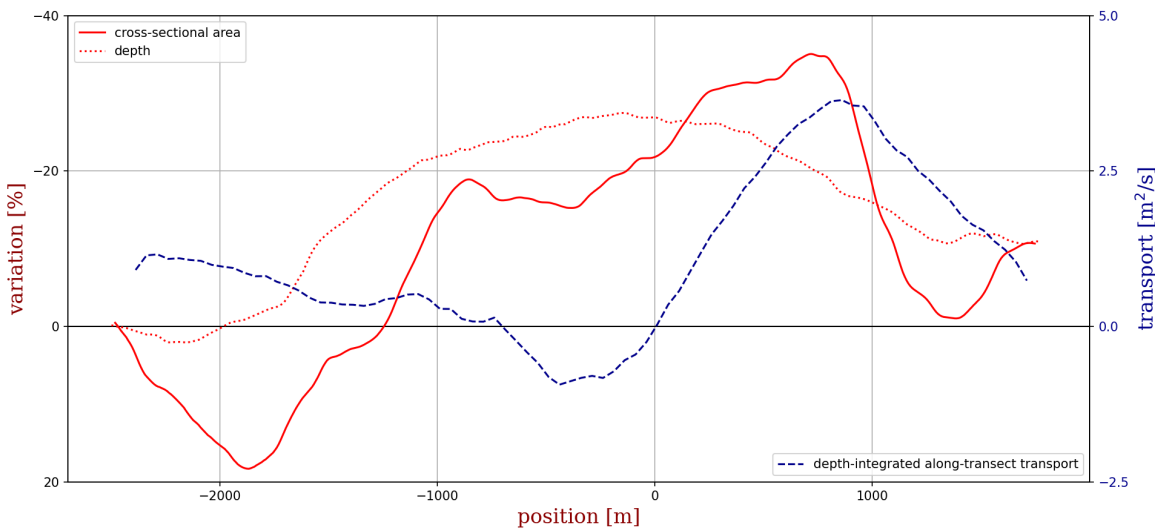


Figure 21: Cross-sectional area and depth variation (red) relative to up-fjord geometry (-2500 m to 2400 m) and depth-integrated along-transect transport (blue) for transect 4 at sill C.

1.6 Conclusion

A schematic summary of the tidal variability of the flow over sills B and C is presented in figure 22.

Sill B

On the flood tide, a downslope flow only forms during the second half of the tide hindering the formation of an internal hydraulic jump. We hypothesize that this is caused by the presence of denser water on the up-fjord side of the sill which results in a density-forced flow separation. On the high tide opposing currents lead to shear-induced instabilities. The ebb tide is characterized by strong currents (at least 0.8 m s^{-1}), the formation of an internal hydraulic jump, and the generation of internal waves at the entrainment interface. When breaking, the internal hydraulic jump becomes an important source of turbulent mixing.

Sill C

On the flood tide, the main flow is located slightly upstream of the crest at $\sim 40 \text{ m}$ depth,

with along-fjord currents reaching 0.6 m s^{-1} . However, strong currents could also lie beneath the zone sampled by the ADCP ($100 \text{ m} < d < 120 \text{ m}$). The ebb tide is characterized by a well-established downslope flow that extends upstream of the crest where it rises above the depth of the sill. At peak intensity, the strongest along-fjord currents are found near the sill face at 0.8 m s^{-1} . On both the high and the low tides, opposing currents lead to shear-induced instabilities.

As expected, our observations showed that sill B is more active than sill C in regards to tidally induced hydraulic processes: upstream and downstream responses, formation of an internal hydraulic jump, and the generation of internal waves. Thus sill B is an important contributor to the mixing of intermediate and outer basin water. However, both sill B and sill C are most certainly hot spot for turbulent mixing.

We found indications that the internal waves observed at sill B are generated at the entrainment interface of the weakly stratified layer on the ebb tide. This provides an additional source of internal solitary waves at sill B to the one identified in [Bourgault et al. \(2016\)](#) that is by the frontal collision of two water masses. No internal waves were observed at sill C thus no evidence was found of internal waves propagating into the inner basin which was suggested by [Belzile et al. \(2016\)](#) as a possible cause of the high mixing rate in the inner basin. However, the relatively short transect line at sill C ($\sim 4.3 \text{ km}$ versus $\sim 5.4 \text{ km}$ at sill B) and small sampling duration (two semi-diurnal tide cycles) don't allow us to conclude that internal waves are not generated at sill C. Furthermore, as previously mentioned, our observations were made during low-energy tide cycles (neap tides) and thus similar experiments are needed to study the formation of internal hydraulic jumps during high-energy tides cycles (spring tides).

Interestingly, we observed the formation of shear-induced instabilities during the reversing of the tides except during the low tide at sill B. This coincides with the seemingly absent exchange flow after the ebb tide at sill B that suggest that the exchange flow plays an important role in the generation of the shear-induced instabilities. Therefore, we hypothe-

size the upstream and downstream responses of the isopycnals are important contributors of turbulent mixing at the sills.

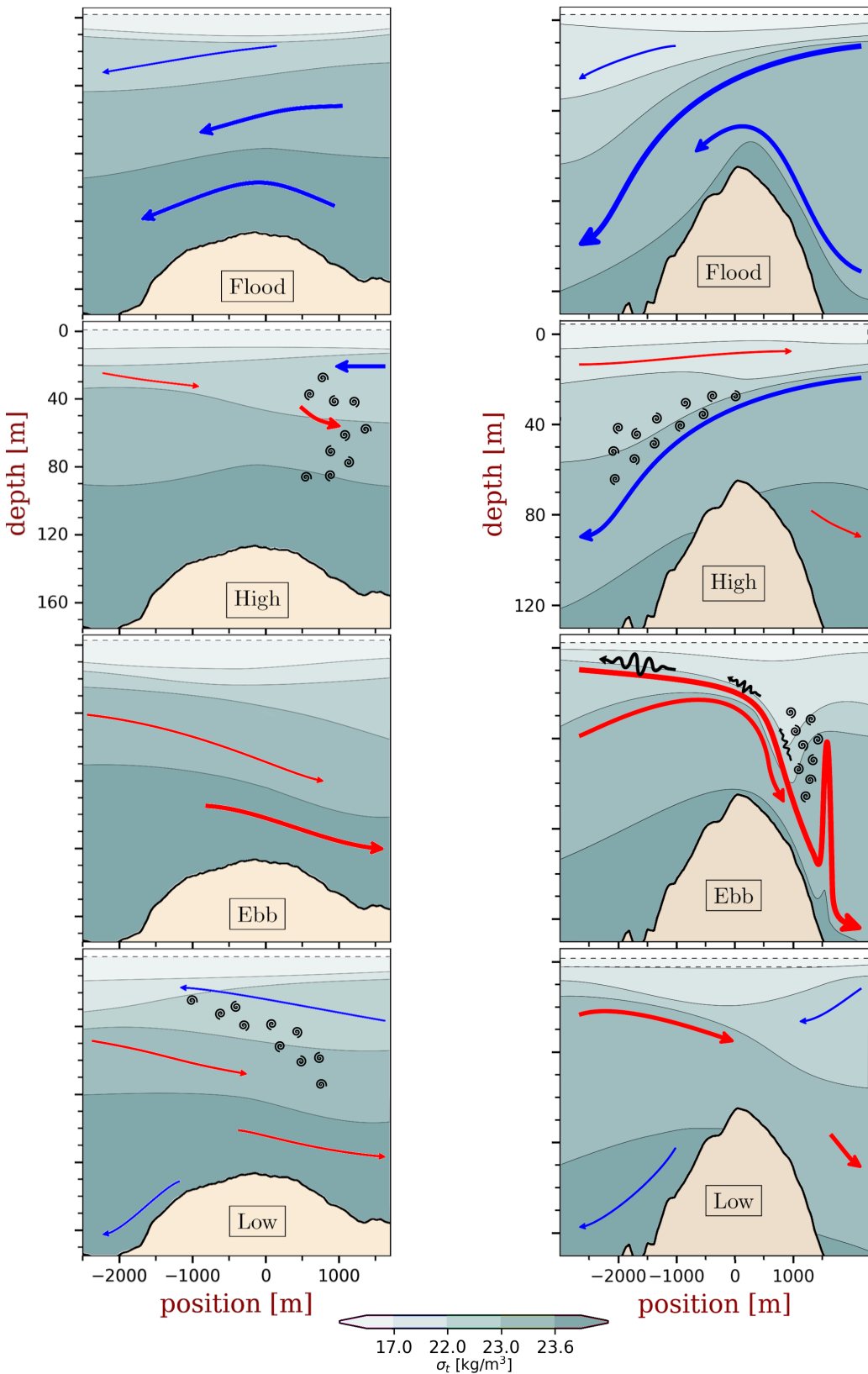


Figure 22: Schematic synthesis of the tidal flow over sill C (left) and sill B (right).

CONCLUSION GÉNÉRALE

Nos observations montrent que le seuil B est plus actif que le seuil C en ce qui concerne les processus de seuils : les réponses de l'écoulement en amont et en aval des seuils, la formation de ressaut hydraulique interne ainsi que la génération d'ondes internes. Par conséquent le seuil B contribue probablement d'avantage au mélange turbulent dans les bassins intermédiaire et extérieur que le seuil C. Nos observations suggèrent également que des ondes internes sont générées à l'interface d'entraînement de la couche faiblement stratifiée qui se forme au seuil B lors du jusant. Ce mécanisme de génération d'onde interne s'ajoute à celui identifié par [Bourgault et al. \(2016\)](#), soit par la collision frontale de deux masses d'eau de surface, qui était jusqu'à présent le seul observé au seuil B. Notons qu'aucune onde interne n'a été observée au dessus du seuil C ou se propageant en direction du bassin intérieur. Toutefois, la ligne de transect relativement courte au seuil C ($\sim 4,3$ km contre $\sim 5,4$ km au seuil B) ainsi que la courte période de mesure (deux cycles de marée semi-diurne) ne nous permettent pas de conclure que des ondes internes ne sont pas générées au seuil C. Nous avons également observé que du mélange turbulent de cisaillement se produit aux seuils B et C lors de l'inversion des marées en raison de la réponse en amont et en aval des isopycnes aux courants de marée. Des études plus approfondies sont nécessaires afin de comprendre l'impact de cycles de marées plus énergétiques ainsi que de la variation saisonnière de la stratification des eaux du fjord sur les processus de seuils.

RÉFÉRENCES

- Bélanger, C., 2003. Observation and modelling of a renewal event in the Saguenay Fjord. Ph.D. thesis. Université du Québec à Rimouski.
- Belzile, M., Galbraith, P.S., Bourgault, D., 2016. Water renewals in the Saguenay Fjord. *Journal of Geophysical Research : Oceans* 121, 638–657.
- Bourgault, D., Galbraith, P.S., Chavanne, C., 2016. Generation of internal solitary waves by frontally forced intrusions in geophysical flows. *Nature communications* 7, 13606.
- Bourgault, D., Galbraith, P.S., Winkler, G., 2012. Exploratory observations of winter oceanographic conditions in the Saguenay Fjord. *Atmosphere-Ocean* 50, 17–30.
- Cyr, F., Bourgault, D., Galbraith, P.S., 2011. Interior versus boundary mixing of a cold intermediate layer. *Journal of Geophysical Research : Oceans* 116.
- Drainville, G., 1968. Le Fjord du Saguenay. I, Contribution à l'océanographie. *Le Naturaliste Canadien* 95, 809–855.
- Farmer, D., Armi, L., 1999a. The generation and trapping of solitary waves over topography. *Science* 283, 188–190.
- Farmer, D., Armi, L., 1999b. Stratified flow over topography : the role of small-scale entrainment and mixing in flow establishment. *Proceedings of the Royal Society of London. Series A : Mathematical, Physical and Engineering Sciences* 455, 3221–3258.
- Galbraith, P., Bourgault, D., Belzile, M., 2018. Circulation et renouvellement des masses d'eau du fjord du saguenay. *Le Naturaliste canadien* 142, 36–46.
- Galbraith, P.S., 2006. Winter water masses in the Gulf of St. Lawrence. *Journal of Geophysical Research : Oceans* 111.
- Galbraith, P.S., Kelley, D.E., 1996. Identifying overturns in CTD profiles. *Journal of Atmospheric and Oceanic Technology* 13, 688–702.
- Gargett, A.E., Holloway, G., 1984. Dissipation and diffusion by internal wave breaking. *Journal of Marine Research* 42, 15–27.
- Klymak, J.M., Gregg, M.C., 2003. The role of upstream waves and a downstream density pool in the growth of lee waves : Stratified flow over the Knight Inlet sill. *Journal of physical oceanography* 33, 1446–1461.
- Lavoie, D., Simard, Y., Saucier, F., 2000. Aggregation and dispersion of krill at channel heads and shelf edges : The dynamics in the Saguenay - St. Lawrence Marine Park. *Canadian Journal of Fisheries and Aquatic Sciences* 57, 1853–1869.

- Long, R., 1970. Blocking effects in flow over obstacles. *Tellus* 22, 471–480.
- Loucks, R., Smith-Sinclair, R., 1975. Report on the physical oceanography of the Saguenay Fjord. Technical Report. Chemical Oceanography Division. Bedford Institute of Oceanography, Dartmouth, N.S.
- Stacey, M.W., Gratton, Y., 2001. The energetics and tidally induced reverse renewal in a two-silled fjord. *Journal of Physical Oceanography* 31, 1599–1615.
- Stigebrandt, A., Aure, J., 1989. Vertical mixing in basin waters of fjords. *Journal of Physical Oceanography* 19, 917–926.
- Therriault, J., De Ladurantaye, R., Ingram, R., 1984. Particulate matter exchange across a fjord sill. *Estuarine, coastal and shelf science* 18, 51–64.
- Therriault, J.C., Lacroix, G., 1975. Penetration of the deep layer of the Saguenay Fjord by surface waters of the St. Lawrence Estuary. *Journal of the Fisheries Board of Canada* 32, 2373–2377.
- Xie, H., Aubry, C., Bélanger, S., Song, G., 2012. The dynamics of absorption coefficients of CDOM and particles in the St. Lawrence estuarine system : Biogeochemical and physical implications. *Marine Chemistry* 128-129, 44–56.
- de Young, B., Pond, S., 1988. The deepwater exchange cycle in Indian Arm, British Columbia. *Estuarine, Coastal and Shelf Science* 26, 285–308.